COMITATO NAZIONALE PER L'ENERGIA NUCLEARE
Laboratori Nazionali di Frascati

LNF-74/51(R)
21 Agosto 1974

S. R. Amendolia, A. Baroncelli, G. Bellini, A. Bertani, E. Bertolucci, G. Bologna, C. Bosio, U. Bottigli, C. Bradaschia, A. Cantore, R. Car, A. Del Guerra, B. D'Ettorre Piazzoli, M. Di Corato, F. L. Fabbri, A. Fiocca, M. Fiori, L. Foà, P. L. Frabetti, A. Giazotto, M. Giorgi, P. F. Manfredi, G. Matone,, G. Matthiae, A. Menzione, F. Orsitto, F. Palombo, P. Picchi, G. Pierazzini, M. Quaglia, P. G. Rancoita, A. Reale, P. Rehak, L. Ristori, S. Sala, L. Satta, A. Scribano, M. Severi, P. Spillantini, P. Stanga, A. Stefanini, G. Vegni, L. Vincelli, R. Visentin and A. Zallo:

THE ITALIAN COLLABORATION AT SPS: FURTHER REMARKS TO THE EXPERIMENTAL PROGRAMME IN HADRON FRAGMENTATION. -

Servizio Documentazione
dei Laboratori Nazionali di Frascati del CNEN
Casella Postale 70 - Frascati (Roma)

Laboratori Nazionali di Frascati del CNEN
Servizio Documentazione

LNF-74/51(R)
21 Agosto 1974

S.R. Amendolia[x], A. Baroncelli[+], G. Bellini[o], A. Bertani[x], E. Bertolucci[x], G. Bologna, C. Bosio[+], U. Bottigli[x], C. Bradaschia[x], A. Cantore[o], R. Car[o], A. Del Guerra[x], B. D'Ettorre Piazzoli, M. Di Corato[o], F.L. Fabbri, A. Fiocca[o], M. Fiori[x], L. Foà[x], P.L. Frabetti[o], A. Giazotto[x], M. Giorgi[x], P.F. Manfredi[o], G. Matone, G. Matthiae[+], A. Menzione[x], F. Orsitto[x], F. Palombo[o], P. Picchi, G. Pierazzini[x], M. Quaglia[x], P.G. Rancoita[o], A. Reale, P. Rehak[x], L. Ristori[x], S. Sala[o], L. Satta, A. Scribano[x], M. Severi[x], P. Spillantini, P. Stanga[x], A. Stefanini[x], G. Vegni[o], L. Vincelli[x], R. Visentin and A. Zallo: THE ITALIAN COLLABORATION AT SPS: FURTHER REMARKS TO THE EXPERIMENTAL PROGRAMME IN HADRON FRAGMENTATION. -

INTRODUCTION. -

In a preceding paper (LNF-74/7; CERN SPS C/P6) we have described the experimental programme of the italian collaboration at the SPS for a comparative study of hadron fragmentation.

In the present paper we go into greater detail on the same programme and we focalize our attention on the following points:

(+) - Physics Laboratory, Istituto Superiore di Sanità, Roma; Istituto Nazionale di Fisica Nucleare, Sezione Sanità.
(o) - Istituto di Fisica dell'Università, Milano; Istituto Nazionale di Fisica Nucleare, Sezione di Milano; Istituto di Fisica dell'Università, Bologna.
(x) - Istituto di Fisica dell'Università, Pisa, Scuola Normale Superiore, Pisa.
(x) - Istituto di Fisica dell'Università, Roma, Istituto Nazionale di Fisica Nucleare, Sezione di Roma.

i) How well and to what extent will the pattern recognition for many--body events be possible?
ii) How will the spectrometer be triggered?
iii) What do we intend to do for particle identification?

In Section 1 we describe further progress made in the design of the apparatus. In Section 2 we discuss a number of features of inelastic diffractive and non diffractive events which can be studied in our experiment, specifying a set of suitable selective triggers. In the same section we also explain the techniques with which we plan to identify the particles involved in the trigger. In Section 3 the possibility of identifying the particles produced in the central c.m. rapidity region is discussed.

Finally, in the last section, we give details of the procedure of event reconstruction, and we quote the results obtained with our analysis programs applied to events generated with the Monte Carlo method.

1. - THE UPDATED SET-UP -

A few modifications have been introduced into the planned set-up. The main changes with respect to the apparatus described in preceding paper are the following:

1.1. - Chamber arrangement in the forward spectrometer -

In P6 we considered locating chambers only in front of and behind each magnet. In order to gain a safety margin in the determination of the (straight) particle trajectories between two magnets, we now plan to insert a further set of chambers in an intermediate position, as shown in Fig. 1. In the region between the vertex detector and the first magnet of the forward spectrometer, two extra sets of chambers have been added.

Each set of chambers consists of an x and y plane of drift wires, each plane providing also a measurement of the other coordinate by means of delay lines parallel to the wires, with an accuracy of a few millimeters.

1.2. - Photon detectors. -

In the original proposal each photon detector consisted of two separate parts, a set of scintillation counter hodoscopes sandwiched by lead plates and a subsequent array of lead-glass counters for the absorption of the remaining part of the shower. While this structure provides the best resolution in energy and angle, it is not well suited for providing a fast trigger on the photon energy or transverse momentum. For this reason, whenever possible, the photon detectors will consist only of lead-

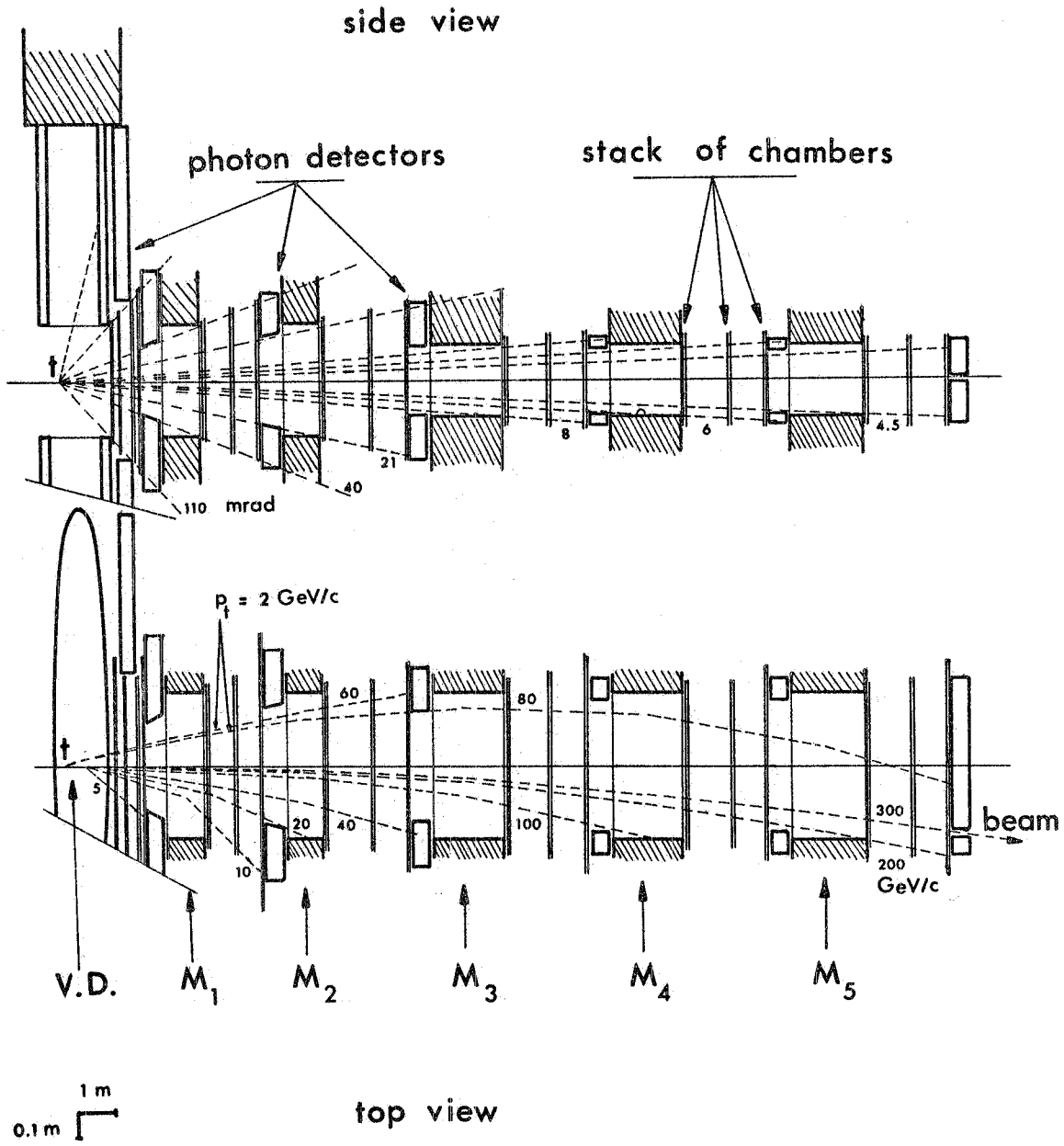

FIG. 1 - General lay-out of the experiment.

-glass counters. This is particularly easy for the last four detectors of the forward spectrometer, where the frame structure of the detectors allows the use of a limited number of counters.

1.3. - Vertex detector. -

The vertex magnet used in the calculation of this addendum is identical to that described in the proposal (see fig. 2). We are, however, considering the possibility of using an existing magnet (at LNF) which, suitably modified, could fit the requirements of our experiment.

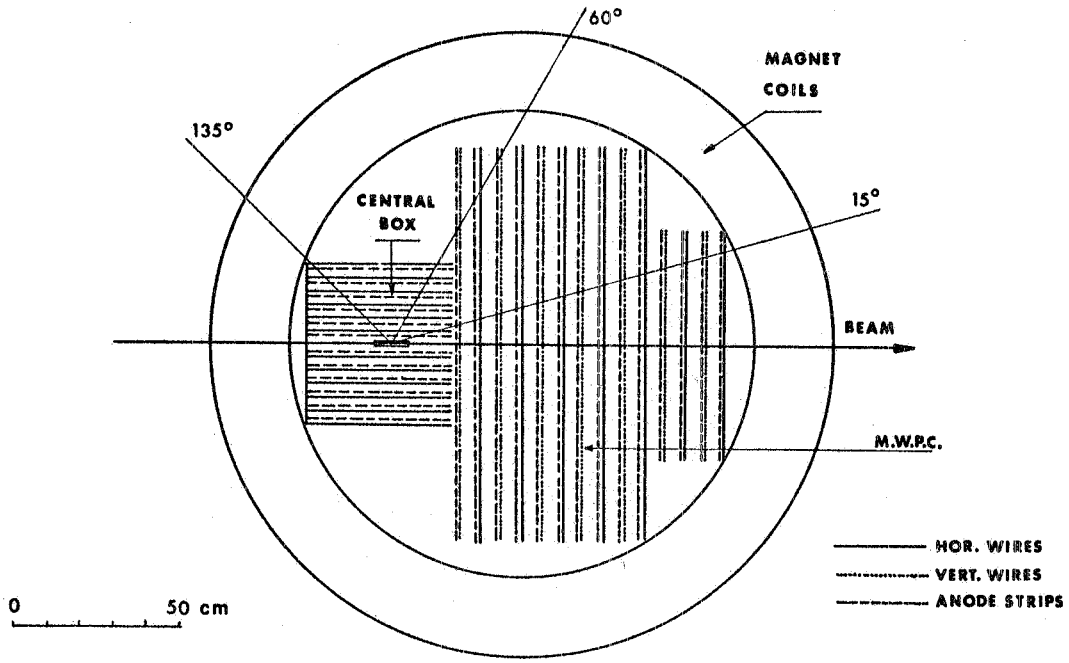

FIG. 2 - Structure of the detectors inside the vertex detector magnet. The MWPC have a rectangular shape, while CB is a set of chambers around the target.

The main part of the vertex detector consists, as described in SPSC/P6, of a set of MWPC orthogonal to the beam. With regard to the position of the target, and of the surrounding chambers, we are considering two options: the first one is to position the target inside the magnet, as explained in the proposal. All calculations on event reconstruction have been made under this assumption. The second one consists in positioning the target immediately in front of the magnet. This geometry excludes from the magnetic analysis the particles produced at an angle larger than $\sim 30^{\circ}$ with respect to the beam, corresponding to a region $\backsim$ 1.5 units wide in rapidity in the target fragmentation cone. As discussed later, in most of the proposed measurements the attention is focused on the projectile frag-

mentation and on the central rapidity region, while in the target fragmentation cone the knowledge of the multiplicity and of the angular distribution of tracks can be sufficient. This solution will be adopted if the large-angle (low momentum) tracks will turn out to be source of difficulties in the pattern recognition.

Finally, we envisage that for special measurements, mainly for the study of the diffractive inelastic component, a streamer chamber, positioned inside the magnet, may be used as vertex detector.

1.4 - Trigger counters. -

In the preceding paper we did not give a description of the trigger counters, since we only mentioned in some detail an inclusive trigger. On the other hand, since we are going to illustrate in the following a set of possible selective triggers, a thorough description of this part of the apparatus is now in order.

The trigger counters are arranged in a number of hodoscopes that cover nearly the whole solid angle and provide a rough measurement of the charged multiplicity of each event.

A set of vertical counters is arranged inside the magnet coils, as shown in Fig. 3a, leaving an aperture in the most forward and backword

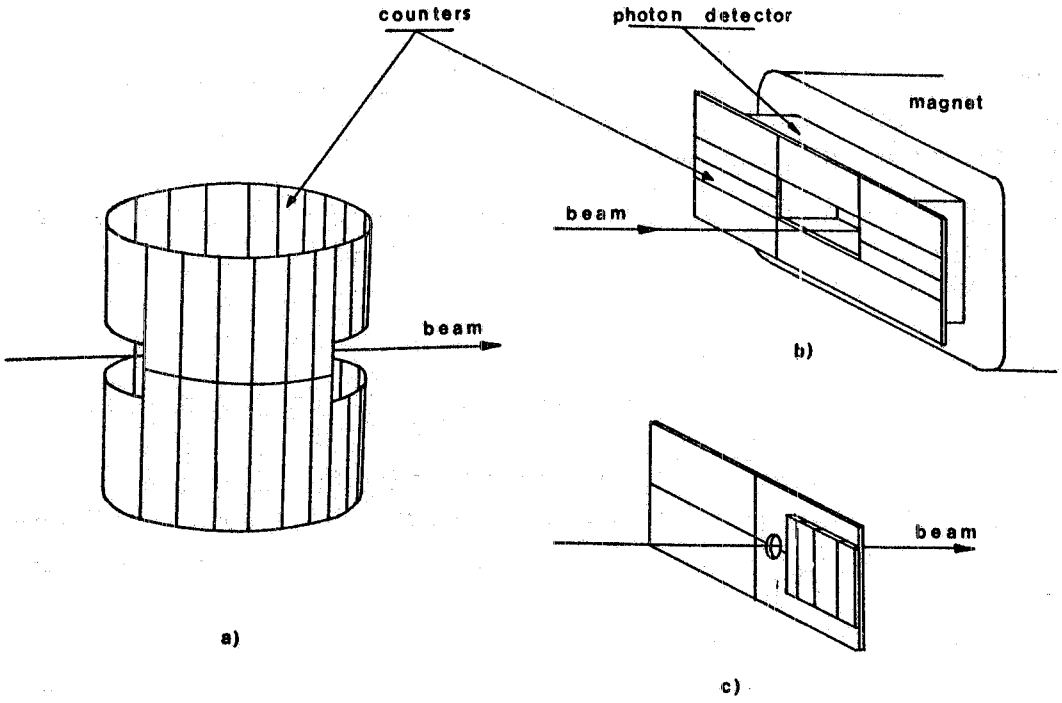

FIG. 3 - Sketch of the trigger counter arrangement inside the V.D. (a); in front of a γ-detector (b); after the last magnet of the spectrometer (c). The counter hodoscope in c) is the trigger for elastic events.

directions(x).

If the solution of an outside target is chosen, an additional counter box will enclose the chambers surrounding the target.

In the forward spectrometer, frames of counter hodoscopes are positioned in front of the photon detectors at the entrance of each magnet, as shown in Fig. 3b. In this arrangement, each hodoscope detects the charged particles which are absorbed by the photon detectors and by the magnet yoke behind it. The average number of particles detected per event by the various hodoscopes is calculated to vary between $\sim$3 (in front of the first magnet) to $\sim$ 0.4 (at the end of the spectrometer). The number of elements in the hodoscopes is scaled according to the expected flux, with the rule that the number of counters is $\sim$10 times the average rate of particles. The relative counter sizes have been chosen in such a way as to equalize their expected rates. Table I gives the number of counters in each hodoscope.

TABLE I

Hodoscope number	Position	Number of counters	Average y_{cm} intervals
1	in vertex detector	32	-4.2 → -1.8
2	in front of M_1	24	-1.8 → -0.6
3	" " " M_2	16	-0.8 → +0.3
4	" " " M_3	8	0.1 → 1.4
5	" " " M_4	8	1.1 → 2.1
6	" " " M_5	8	2.0 → 2.8
7	behind M_5	4	2.7 → 4.2

In front of the last photon detector of the forward spectrometer, an additional set of scintillation counters provides a trigger for elastic events. These counters are shown in Fig. 3c.

Finally, two sets of counters will be placed on the beam, in front of the target and at the end of the spectrometer, and will be used to provide an IN-OUT inclusive trigger.

2. - EXPERIMENTAL PROGRAMME AND SELECTIVE TRIGGERS -

In the following we describe the main physics items that we plan to study in addition to the inclusive properties of inelastic events as discussed in SPSC/P6, and for each of them we specify a set of possible selective triggers.

(x) - The geometry of these counters will have to be somewhat modified when the streamer chamber is used as a vertex detector, since this chamber extends also between the coils.

2.1. - Non-diffractive component correlations and clusters. -

The study of high-energy multibody production at the ISR and at FNAL has shown that strong two-body correlations exist among the secondaries. Both long - and short-range correlations are simultaneously present and cannot be separated in a model-independent way in a pure inclusive measurement. While long-range correlations are mainly connected with phase-space effects and with the presence of , at least, two different production mechanisms (diffractive and non-diffractive components), the short-range correlations provide a powerful tool for studying the dynamics of multibody production. Recent results on correlations inside events of fixed charged multiplicity show that a very simple interpretation of these data can be given in terms of cluster models. It is not yet clear whether these clusters correspond to real objects produced in an early stage of the interaction or whether they are just a convenient phenomenological description of the production mechanism.

We are mainly interested in the study of correlations and clusters in the central c.m. rapidity region in order to check to what extent they depend on the nature of the projectile and inside the projectile fragmentation cone, where a more direct memory of the nature of the parent particle should be felt.

To perform these studies, we plan to do the following measurements:

i) a simultaneous measurement of y and $\vec{p}_T$ correlations;
ii) the measurement of the charged and neutral multiplicity of each event;
iii) the indentification of the mass of one (or more) of the particles produced, mostly in the central c.m. rapidity region.

The first measurement will allow a more direct signature of clusters as real objects, if transverse momentum correlations will be found for particles contained in approximately one correlation length in rapidity.

Information on the event multiplicity has been shown to be of fundamental importance in order to separate the non-diffractive from the diffractive events. By selecting events with $n_{ch} \geq \langle n_{ch} \rangle$ or with a few particles in the central rapidity region, the diffractive component will be eliminated and the structure of short-range correlations in pionization events will be studied in detail.

The measurement of the mass of the produced particles will allow a deeper study of the mechanism of cluster decay. For instance, one may argue that the correlation length associated with kaons and protons should be smaller than that associated with pions, if the cluster decay is isotropic.

Although the above-mentioned studies could be carried out in part with an inclusive trigger and a suitable off-line analysis, a number of simultaneous selective requirements must be put on the events at the trigger level if we want to be able to collect the amount of statistics which is needed for correlation studies.

In the following we describe a list of possible triggers which can be used to enrich particular samples of events.

2.1.1. - Selection of event multiplicity in the trigger. -

The signals from the counter hodoscopes can be used to trigger on events of fixed charged multiplicity, and the same selection can be done on the photon multiplicity by means of the photon detectors. A combination of these two items of information allows triggering on the total event multiplicity. These triggers can be extended to the whole solid angle or restricted into definite regions of space. Table I shows the intervals of c.m. rapidity y^* covered by the various counter hodoscopes for pions, as obtained in our Monte Carlo calculation (see Section 4). The program was run at p_{inc} = 300 GeV/c and the spectra were averaged over p_T. Since these intervals are reasonably separated, the requirement of fixed multiplicities in particular regions will allow the collection of large statistics on events of definite topology and of small cross-section, such as, for instance, double diffractive events.

Since the space resolution of the counter hodoscopes is modest, a fixed measured multiplicity will correspond to a number of true multiplicities at the production ($\pm$ 2 units around n_{ch}). Based on the clearer information from the chambers, the requirement of fixed multiplicity will be sharpened in the off-line analysis.

2.1.2. - Trigger on photons of fixed transverse momentum. -

An angle-dependent pulse-height discrimination of the signals from the photon detectors allows filtering of photons of fixed p_T, regardless of the angle at which they are emitted. This requirement can be set in the trigger and possibly added to the above-mentioned conditions on event multiplicity. We can thus study the correlation function $C_{(n)}[y_\gamma^*, \vec{p}_{T_\gamma}; y^*, \vec{p}_T]$ between photons and other particles as a function of the longitudinal and transverse variables.

This trigger illustrates an important feature of the proposed set-up in which one is able to obtain at the same time a full coverage and thus a complete picture of the event, and the highly selective trigger which is necessary for the study of low cross-section processes. One can change the specific trigger according to almost any physics requirement, without losing this property.

2.1.3. - Trigger on fixed E_γ -

An interesting and very selective trigger can easily be built by selecting the events according to the amount of energy carried by the photons. In particular we can trigger on rare events in which the large majority of the energy has been transferred to the photons. Since the photon multiplicity is also measured, we can further select many - photon events from events in which only one hard photon has been produced.

2.1.4. - Trigger on identified particles at $y^* \cong p_T \cong 0$. -

Particles of different mass, produced in the central rapidity region with p_T close to zero can be identified by means of a simple telescope of two Čerenkov counters placed behind the first magnet of the forward spectrometer. The study of two-body correlations in the central region can then be performed for various combinations of projectiles and of produced particles.

The experimental arrangement for this trigger is shown in Fig. 4 at $p_{inc} \equiv 300$ GeV/c and for two different positions. The counter $\check{C}_1$ is filled with N_2 and is sensitive only to pions up to 20 GeV/c. Counter $\check{C}_2$ is filled with freon and is sensitive to kaons for $p \geq 10$ GeV/c. Assuming the dimensions of the counters to be 10 x 10 x 180 cm^3 for $\check{C}_1$ and 15 x 30 x x 80 cm^3 for $\check{C}_2$, we have calculated the expected rates for π's to range between 0,1 and 0,2 particles/event. In order to be able to span a larger rapidity interval, magnet M_1 has been supposed to be of C-type.

Fig. 5 shows, as an example, the momentum band of particles entering the Čerenkov counter telescope when this is in the positions of Fig. 4. By moving the telescope at intermediate positions, we can cover an important byte of the central rapidity region, while maintaining a clean separation of π's, K's, and protons. The y^*-regions in which the different particles are separated are shown in Fig. 5.

Since the Čerenkov counters are small and are operated at atmospheric pressure, their construction is simple and they can be made very light. Because of the fact that the mean multiplicity in these counters is well below one, the momentum measurement of particles to be analysed between M_1 and M_2 is not appreciably perturbed.

2.1.5. - Trigger on identified fast particles. -

The identification of a leading fast particle can be performed at the end of the spectrometer by means of a long Čerenkov counter. It is even conceivable that in four years' time the present development of radiation transition detectors will allow the construction of a much smaller, counter able to identify particles in the hundred GeV region. The insertion of such a detector in the experiment would make it possible to perform many interesting measurements on the properties of Regge poles by selecting suitable combinations of projectiles and forward-produced particles.

2.1.6. - Study of the diffractive component. -

On the basis of the first ISR and NAL results one of the important subjects of the future work at the SPS will be the study of the diffractive component in inelastic hadron collisions.

Diffractive events are qualitatively understood as the excitation of one of the interacting hadrons, while the other hadron remain unexcited.

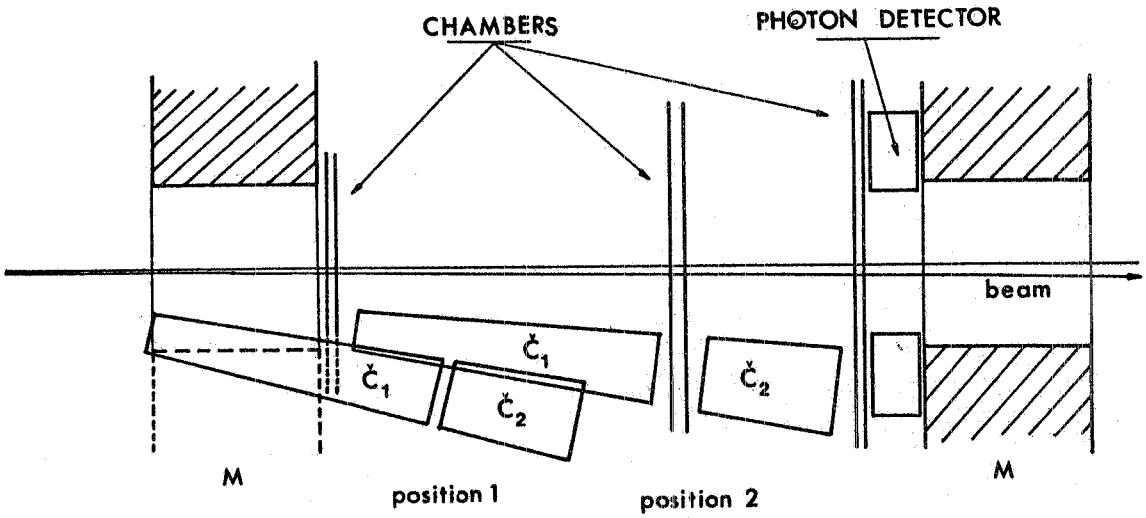

FIG. 4 - Two possible experimental arrangement, 1 and 2, for triggering on identified particles at $y^{*} \simeq p_T \simeq 0$.

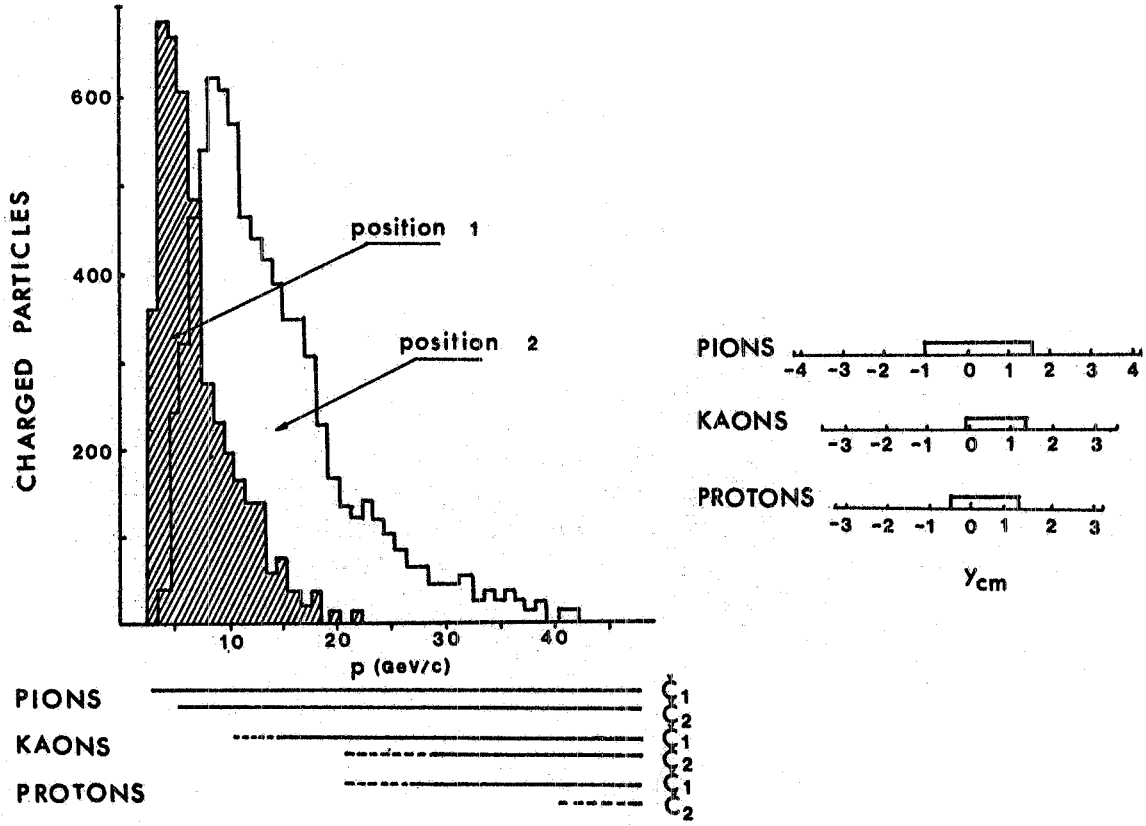

FIG. 5 - Momentum distribution of the particles identified in the Cerenkov counters. The shadowed distribution refers to arrangement 1, the not shadowed one to arrangement 2, in Fig. 4.

The study of the clustering properties of the particles produced in inelastic collisions at the ISR suggests that events of this type are very abundant and that the produced particles are the decay products of some heavier object which moves along the same direction as that of one of the primary particles.

More detailed properties of this phenomenon have been derived from the study of the inclusive spectrum of protons produced in inelastic events. This spectrum shows at small angles a sharp peak at the boundary of the phase space. The associated bump in the missing-mass spectrum has a tail extending to fairly large masses, whose shape is given approximately by

$$d\sigma/dM^2 \propto 1/M^2.$$

Further studies of this process are needed in order to measure its total cross-section, which in a Regge-pole picture of hadronic interactions is supposed to increase logarithmically with the energy. This hypothesis is particularly attractive because it can explain the experimental fact that all hadronic total cross-sections increase above $p_{inc} \simeq$ $\simeq 100$ GeV/c. In the framework of this model, accurate measurements of the total diffractive cross-sections with different incoming projectiles would also provide information on the factorization properties of the Pomeron couplings. Furthermore, by extending the measurements at very low $|t|$ values one can check whether the triple Pomeron amplitude decouples at $|t| = 0$. Needless to say, the comparative study of the excitation properties of different hadronic projectiles is an essential feature of this experiment.

In the existing experiments the study of the diffractive component becomes ambiguous when the analysis is extended to high values of M^2 or $|t|$, because the identification criteria fail to disentangle diffractive events from the remaining part of the production. As a consequence, no reliable result has yet been obtained on the energy dependence of the total diffractive cross-section. In our experiment we propose to make simultaneous use of both missing-mass and clustering techniques, implemented if necessary by further constraints. To achieve this aim, the following conditions are necessary:

i) the recoiling nucleon must be identified and momentum analysed;
ii) it must be checked that no other particle is produced with longitudinal momentum close to the target nucleon momentum;
iii) the energy of the charged and neutral secondaries associated with the excited mass decay has to be measured in order to reconstruct (even if roughly) the value of the mass and of the transverse momentum of the excited cluster.

We also note that for large values of the produced mass a stronger selection criterion must be used to identify the diffractive events. This additional signature can be obtained if the projectile is excited in nuclear coherent interactions

$$h + M \rightarrow h^{*} + M.$$

It is possible, as discussed later, to use sensitive targets in which the coherence of the interaction can be checked event by event.

2.2.1. - Vertex detector. -

In the study of the diffractive production on H_2, D_2, and He we plan to use as vertex detector a streamer chamber inserted in the vertex magnet. The chamber, whose dimensions are 1 x 1 x 0.3 m^3, has the electric field parallel to the magnetic field. With the chamber, in addition to localizing the interaction point, one can detect the recoil proton and select events without any other charged prong possibly associated with the target fragmentation. Minimum ionizing particles in the forward jet will not be studied inside the chamber. A description of the streamer chamber is given in Appendix 1.

In the study of diffractive production on H_2 it would be ideal to operate the streamer with the same gas which acts as a target, in order to reach very low values of the detected recoil momenta, i.e. very low values of $|t|$. A development study is now in progress for operating a H_2/D_2 streamer chamber by collecting the light produced in the ultra-violet region. It must be pointed out, however, that a more conventional streamer with a H_2/D_2 target inside can be used as well. In Appendix 1 a comparison of the relative merits of the He and H_2/D_2 chambers is given.

For deuterium and helium the coherence requirement limits the useful $|t|$ range to $|t| \leq 0.1\ (GeV/c)^2$, because the cross-section is dominated by the nuclear form factor. At low energy this limitation severely cuts the available mass range, since the minimum longitudinal momentum transferred to the target needed to excite the projectile to a mass M is given by

$$q_{\parallel} = \frac{M^2 - m^2_{proj}}{2p_{proj}}$$

The high energy of the SPS allow the missing-mass measurement to be extended over a large mass interval. Table II shows the values of M for which

$$\frac{d\sigma}{dt}(t_{min}) / \frac{d\sigma}{dt}(t = 0) = 1/e$$

for deuterium and helium.

TABLE II

p (GeV/c)	M (D) (GeV)	M (He) (GeV)
100	7.1	6.3
200	10.0	8.9
300	12.3	11.0

Detail on the momentum and angle resolutions that can be achieved with a streamer used as vertex detector are given in Appendix 1. With these figures we obtain the $|t|$ and M resolutions shown in Figs. 6 and 7 for hydrogen, deuterium, and helium.

Selective triggers may be used to enhance the rate of diffractive events. Basically these triggers will require more than one particle in the trigger counters of the forward spectrometer. The information gathered from the trigger counters in the vertex detector will be used in different ways according to the different kinematical conditions as described in Appendix 1, where we also discuss the criteria used to identify the recoiling particle.

2.2.2. - Study of interactions with nuclei. -

The spectrometer proposed is well suited to study inelastic interactions of hadrons on nuclei. This chapter of physics has lately received great attention because of unexpected features shown in a number of experiments, e.g.

i) the average charged multiplicity in emulsion is only 1.7 times greater than the average multiplicity in hadron-hadron interactions;
ii) the production in the forward cone, containing about one half of the secondaries in a p-p collision, does not depend on the size of the involved nucleus nor on its excitation mode;
iii) the production rate at larger angles seems to depend on the degree of nuclear excitation but not on the atomic number.

It is clear that these phenomena cannot be explained in the framework of a simple cascade model in which projectile and secondaries interact sub

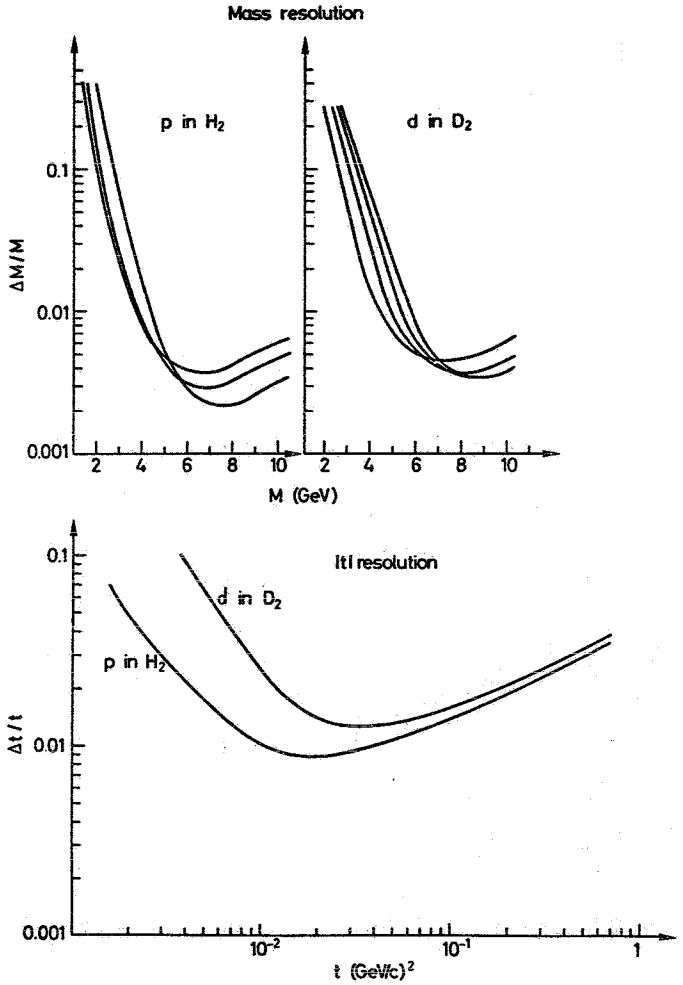

FIG. 6 - $\Delta M/M$ and $\Delta t/t$ resolution that can achieved in a H_2 and D_2 streamer by missing-mass technique using the gas of the chamber as target. M is the mass of the excited incident hadron.

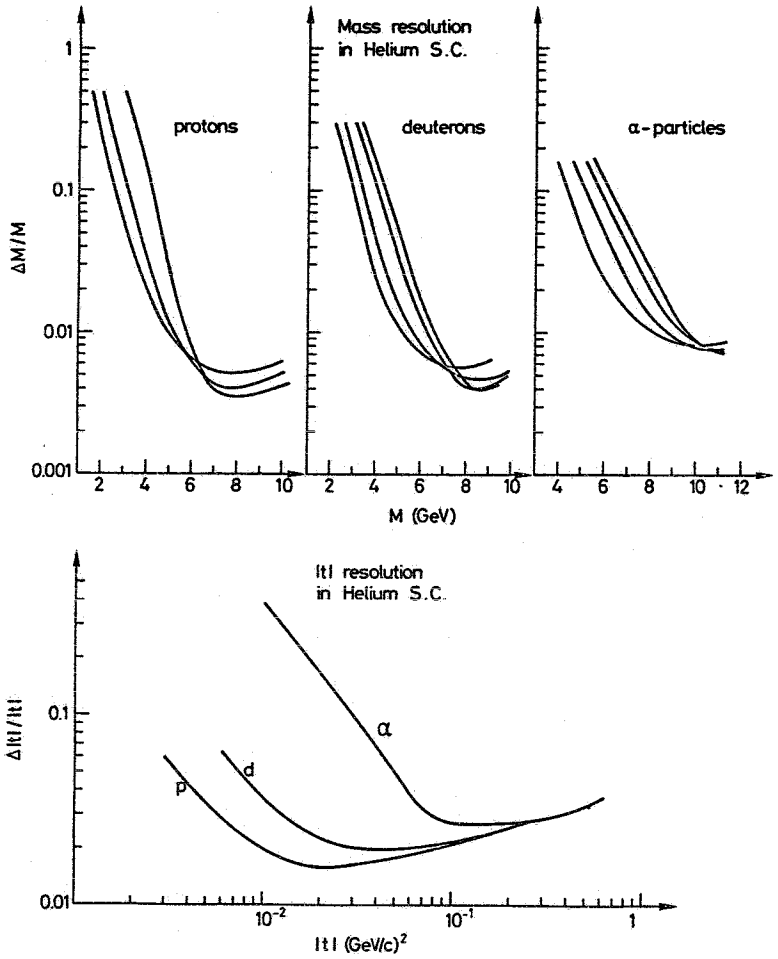

FIG. 7 - Same Fig. 6 but using different targets inside on the streamer chamber.

sequently and independently with the bound target nucleons. It has recently been suggested that these peculiar features of hadron interactions with nuclei may be due to the space-time development of the hadronic two-body interaction.

Therefore to measure the cascade structure as a function of atomic number might be a powerful tool for studying the hadronic interaction in its very early stage of development.

Since no separation between coherent and incoherent events is needed in order to study these interactions, the trigger only requires a jet in the forward spectrometer. These measurement can be performed with various nuclear targets, covering the full range of atomic number, using the standard MWPC detector in the vertex magnet. For each nucleus, energy, and projectile, we can measure with high statistics the multiplicity, the angle, and the momentum spectra of secondaries and make a comparison with the results obtained with hydrogen. In a later stage of the experiment, we plan to study the coherent and incoherent interactions separately. This can be done by means of active targets, sensitive to the recoil of the whole nucleus, of the silicon detector type described in Appendix 2. At present, members of our collaboration are developing active targets consisting of thin metallic layers interspaced with small MWPC in which the nucleus break-up is identified.

3. - PARTICLE IDENTIFICATION -

As discussed in the previous sections we are interested in using identified particles in the triggers as probes for particular processes. Specifically we have treated the following cases:

1) coherently recoiling nucleons or nuclei for the study of the diffractive component (Section 2.2.1);
2) single or multiple photons in the correlation studies (Section 2.1.2.);
3) pions, kaons, and nucleons with $p_T \simeq 0$, to study correlatiohs in the central rapidity region (Section 2.1.4);
4) fast pions, kaons, and nucleons in the forward fragmentation cone (Section 2.1.5), to study the leading particle effect. In these measurements the detailed information on the probe particle will be coupled with nearly complete information on momentum and production angle of the remaining secondaries, in such a way as to allow, we believe, a detailed study of the production mechanism even without the identification of the mass of all particles. In any case it is known by now that most of these particles ($\sim$90%) will be pions.

However, it is possible that the results of the next few years will increase the interest in a more complete identification of the particles produced in each event. In view of this possibility we have studied the compatibility of multicell Čerenkov counters with the present layout of our

forward spectrometer. However, we have not performed any detailed study of the structure of these detectors. If one adops counters $\check{C}_1$ and $\check{C}_2$ of the type described in the North Area Multiparticle Spectrometer White Book, a possible layout is as shown in Fig. 8.

A Čerenkov counter $\check{C}_1$ (80 cm long filled with C_2H_5), is inserted between the vertex detector and the first magnet of the forward spectrometer. Its lateral dimensions, in particular the vertical one, can be strongly reduced with respect to the N.A.M.S.W.B. design, and its central region, which is crossed by fast particles, should be made blind. A similar counter, $\check{C}_2$, and a larger one, $\check{C}_3$ (180 cm long and filled with N_2) are positioned between the first and the second magnet (Fig. 8).

Counter $\check{C}_1$ identifies pions from $\sim$ 2 to $\sim$ 10 GeV/c, while kaons and protons are not seen. They could be separated only by means of a Čerenkov counter working at high pressure, which would strongly decrease the precision of the momentum measurements. Between 10 and 15 GeV/c, pions and kaons are ambiguous, while protons can be identified by the absence of a Čerenkov signal.

4. - PATTERN RECOGNITION -

In the last months we have concentrated our efforts on studying the pattern recognition problems and on a general understanding of our capability for handling many-body events. With this aim in view we have simulated our experiment in a Monte Carlo calculation, in which realistic events are generated and the produced particles traced through the detectors. Unstable particle decays, secondary interactions, and multiple scattering are properly accounted for. The detection of the photon component, because of its greater simplicity, has not been accounted for at this stage. A subsequent reconstruction program uses the information gathered in the chambers to identify the coordinates of the hits, and finally associates them into tracks with the aim of reconstructing the full event.

The Monte Carlo program is described in some detail in the first part of this section. On the basis of the results of these calculations, in the second part the adopted reconstruction procedure is discussed.

4.1. - Simulation of the experiment. -

The first routine specifies the beam energy, momentum acceptance (typically 1%) and divergence (0.1 mrad), the target dimensions, and the geometry of the apparatus. The interaction point is chosen randomly in-

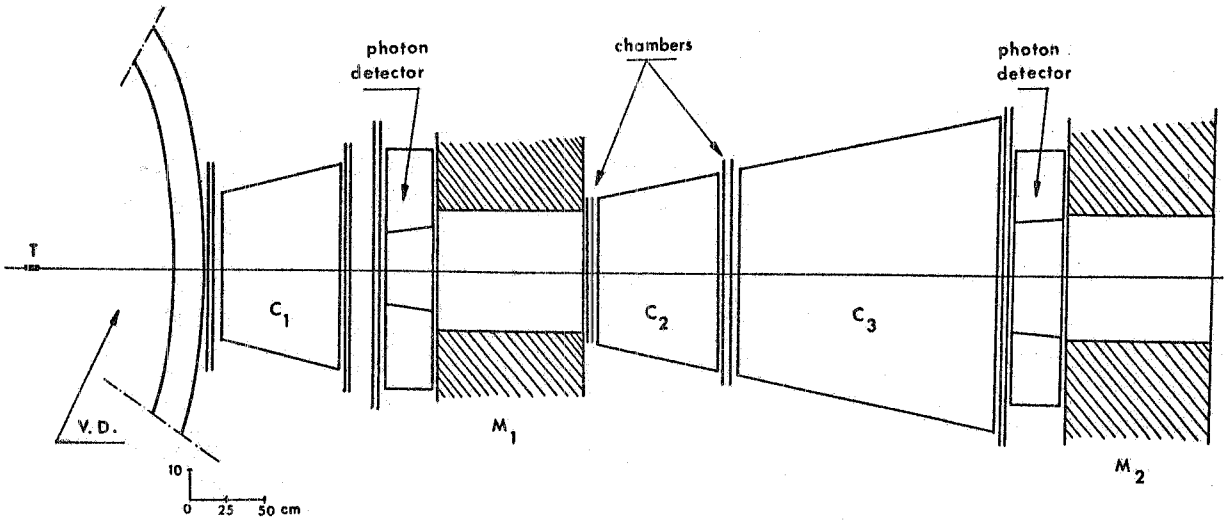

FIG. 8 - Possible layout of Cerenkovs which may be used for particles identification.

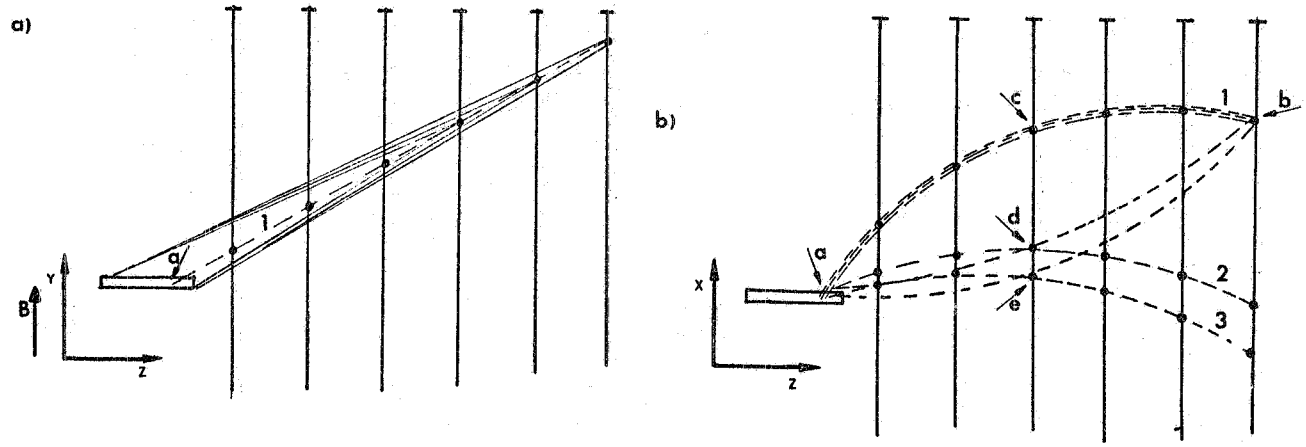

FIG. 9 - Reconstruction technique of a event in the V.D. : a) criteria to identify tracks in the vertical projected plane and determination of the interaction point (a); b) shows how starting pion points b and a the track number 1 is identified resolving the ambiguities due to points d and e in the horizontal projected plane.

side the target. The magnetic fields are taken to be homogeneous and without fringing field. We have checked that this approximation has no appreciable influence on the final results(+).

In the second routine, events are generated according to various production processes:

a) elastic events are produced in proton-proton scattering;
b) diffractive events are generated with a mass distribution $\propto (1/M^2)$ and a $|t|$ distribution $\propto e^{bt}$;
c) pionization events are generated according to what is known at present about multibody production processes. The multiplicity, rapidity, and transverse momentum inclusive distributions are taken from the ISR and NAL results.

Different $d\sigma/dy$ are given in input according to the event multiplicity. However, energy and momentum are conserved only to $\pm$ 20%. As a check of the influence of the poor accuracy of energy-momentum conservation, a sample of events has also been generated according to a model in which energy and momenta are exactly conserved. The y and p_T distributions are calculated according to a multiperipheral model, with in addition a correct reproduction of the momentum distribution of the two leading particles. We have found that we can reconstruct these events, as well as the events generated in the routine mentioned above.

4.2. - Tracking of particles through the apparatus. -

The events mentioned above in Section 4.1 are generated in the c.m. system. After transformation of all secondaries to the laboratory frame, one allows for the decays $\pi^o \rightarrow \gamma\gamma$ and $K_s^o \longrightarrow \pi\pi$. Each particle is then followed in its path through the detectors, until it is absorbed by the coils of the vertex magnet or by a photon detector or by the yoke of a magnet. Photon conversion into electron pairs and δ-ray production in the various materials are taken into account in order to check the level of confusion that these processes might cause in the reconstruction of the charged tracks.

4.3. - Track sampling in the chambers. -

The coordinates of these impact points in the chamber, as found in the routine 4.2 above, are transformed into signals in the nearest wires of the chambers.

For the MWPC of the vertex detector the final information consists of

---

(+) This is due to the fact that particle trajectories are sampled either inside a uniform field (in the vertex detector) or outside small-gap magnets (in the forward spectrometer).

the code numbers of the wires fixed in each chamber.

In the present calculation we have assumed the use of seven x-y chambers 12.5 cm apart, the wire spacing being 2 mm. Induced pulses are also produced on the anode electrodes, suitably split into narrow ($\sim$1 cm) strips. We plan to use these signals, possibly in hardware, to associate the vertical and horizontal coordinates of the sparks. This technique should in principle give the same results as the one using the delay line, parallel to the wires of the drift chambers (see Section 1.1.). If, however, this technique should not work, standard crossed planes of MWPC will be used.

For the drift chambers of the forward spectrometer one measures the drift time of the electron cloud in the gas, T_1, and the two times required by the induced signals to reach the end of the delay line T_2, T_3, which depend on the coordinate along the wire as well as on the electron drift velocity v_D and on the signal propagation velocity in the line v_L. We have taken

$$v_D = 0.1 \text{ mm/sec}$$

and

$$v_L = 1 \text{ mm/sec}.$$

T_1 and T_2, T_3 were spread with a resolving rime of $\pm$ 2 nsec and $\pm$ 5 nsec, respectively. A dead-time of 20 nsec has been associated with each signal.

Accidental signal losses, random firing of wires, detection of out-of-time tracks have been added at the typical level of chambers operating at present.

4.4. - Track reconstruction in the vertex detector. -

The reconstruction procedure adopted for particles detected inside the vertex magnet relies heavily on the high uniformity of the magnetic field. These conditions allow us to treat the horizontal projections (xz plane) as circles and the vertical projections (yz plane) as straight lines(x).

The two projections are studied separately, and the only common information is the longitudinal coordinate of the interaction point which is provided by the vertical projection. In about 10% of the events a more precise measurement of this coordinate should be obtained by means of

(x) - Only for very low momentum particles (below 500 MeV/c) can the helicoidal shape of the trajectory produce a sinusoidal projection on the vertical plane. These particles are analysed with a separate and more sophisticated routine.

the chambers surrounding the target. Supplementary information on the vertex point comes from the first chambers of the forward spectrometer, which compensates the larger distance with a better resolution.

In the vertical plane, the association of the measured coordinates into tracks proceeds as sketched in Fig. 9a. Starting from a spark in the last chamber, the corresponding spark in the preceeding chamber is searched for inside a triangle having the spark as vertex and the target as basis, and so on. When two or more sparks are found in the scanned interval, the most external spark is assumed to belong to the track, since the trajectories never cross each other in the vertical projection. Particles falling into a vertical interval of $\pm$ 40 mm around the beam are not detected since they are clearly analysed in the forward spectrometer. The remaining isolated sparks can be further analysed in order to identify particles not coming from the target (for instance K^0_S decay).

The best value of the z-coordinate of the origin point is then calculated by averaging all values obtained in the analysis of single tracks. The spectrum of the reconstructed origin is shown in Fig. 10 for all events and for completely reconstructed events separately. The width is of $\sim \pm$ 0.5 cm.

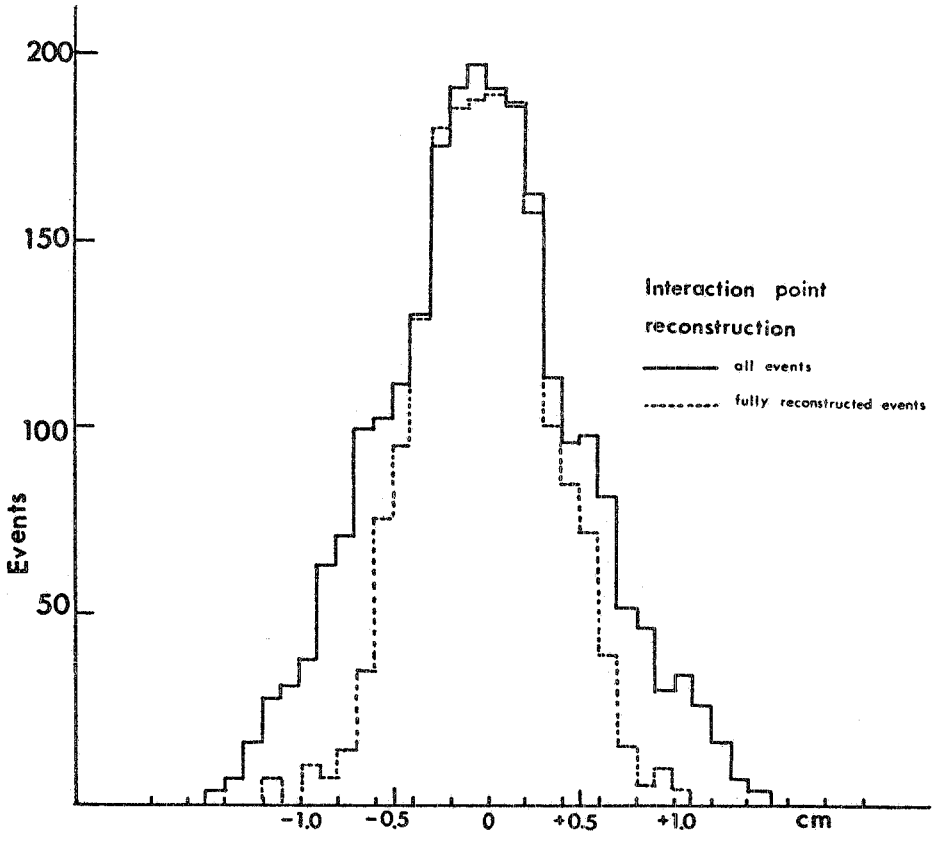

FIG. 10 - Interaction point reconstruction. In abscissa are plotted the differences between the Monte Carlo generated interaction point and the reconstructed one.

A sketch of the reconstruction procedure followed in the horizontal plane is given in Fig. 9b. Beginning again from the last chamber, all circles passing through this point, the interaction vertex in the target, and the sparks in an intermediate chamber, are calculated. The circle collecting more sparks (at least two) in the remaining chambers is identified as a track. The analysis is then repeated starting from all sparks outside an interval of $\pm$ 150 mm around the beam.

Figure 11 a) shows the efficiency for track reconstruction obtained with this method. About 90% of the tracks are correctly reproduced. The efficiency depends only on the multiplicity in the vertex detector and not appreciably on the overall multiplicity of the event.

The efficiency for reconstructing the events, for what concerns the particles contained in the vertex detector, is shown in Fig. 11 b). The efficiency varies between 90% and 70% over the range of multiplicity measured in the vertex detector. If we accept also events in which only one track is badly reconstructed, the efficiency varies between 100% and 90%. We believe that the large improvements which can be introduced in the program should allow a full reconstruction to be reached for all these events.

The presence of spurious sparks (two per event and per chamber) in the chambers does not alter the efficiency of reconstruction. This is shown by the equality of the full curves of Figs. 11b) and 12. An inefficiency of 10% on all wires reduces, however, the percentage of reconstructed events. The $\Delta p/p$ and $\Delta\theta_{xz}$ resolutions are plotted, for various samples of events, in Figs. 13 and 14.

For each event the longitudinal and transverse component of the reconstructed momenta are summed together and compared with the same quantity calculated for the generated event in Figs. 15 and 16. For events in which no particle is lost, the average widths are $\pm$0.12GeV/c in the transverse direction and $\pm$ 0.5 GeV/c in the longitudinal direction.

4.5. - Track reconstruction in the forward spectrometer. -

The knowledge of the three TOF values allows the reconstruction of the position of the spark in the chamber with asymmetric errors ($\pm$ 0.2 cm perpendicular to the wire and $\pm$ 1 cm along the wire). Ambiguities, arising when more than one particle is detected by the same wire, are solved by requesting that the measured times are in the right relation for the particular wire length. Once the right association of times is found, the typical left-right ambiguity of the drift chamber is solved by comparing the coordinates in one plane with those of the orthogonal one. The particle position is identified using a χ^2 fit. It no satisfactory solution can be found, the hypothesis is made that the hit was out of time. In Figs. 17, 18 and 19 we show the number of hits reconstructed with this procedu

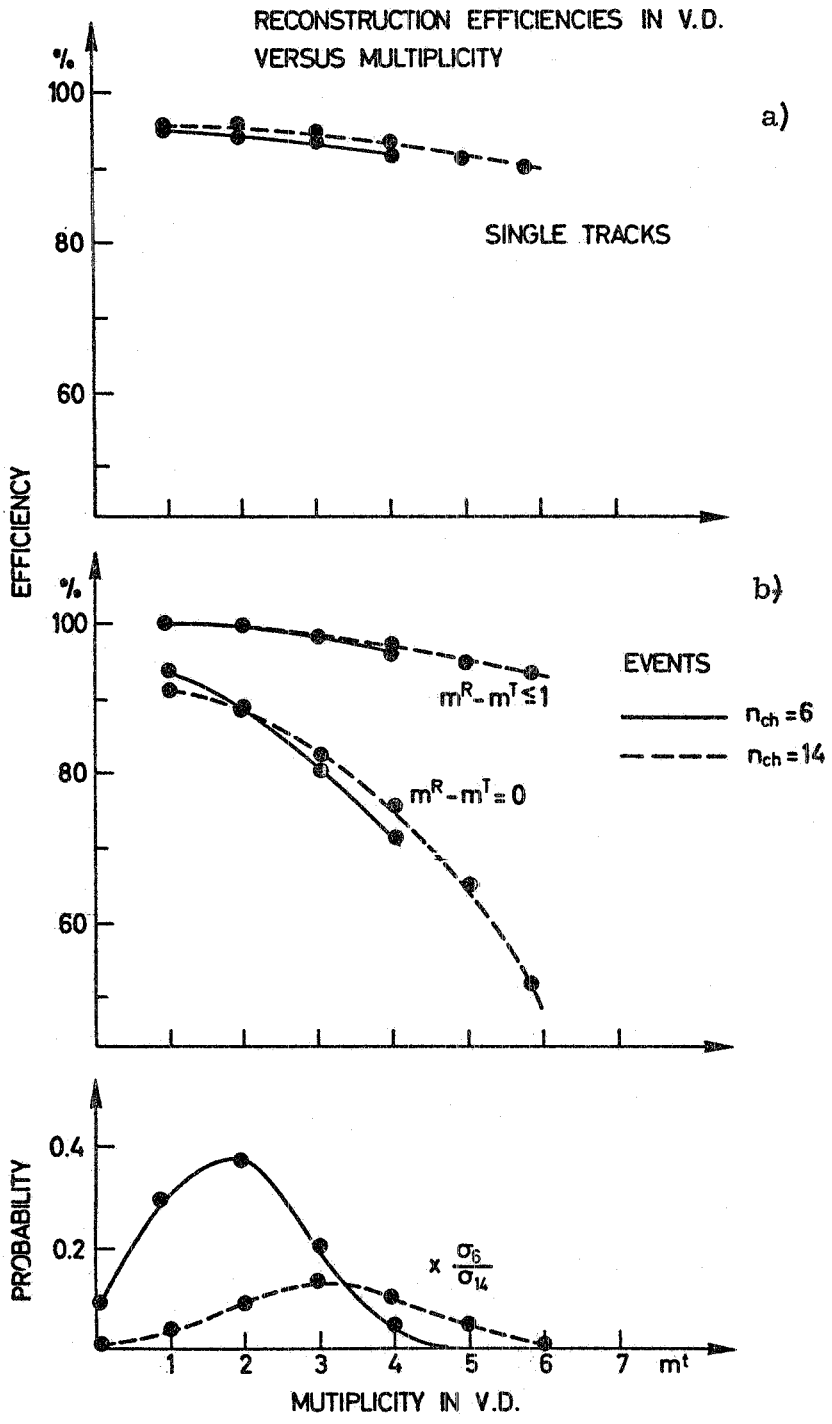

FIG. 11 - Reconstruction efficiency versus multiplicity of tracks (a) and events (b). Full line refers to events with charged multiplicity equal 6, broken line to charged multiplicity equal 14. Fully reconstructed events are indicated by $m^R - m^T = 0$. We show also the multiplicity probability in vertex detector for the two kinds of events weighted with relative cross sections.

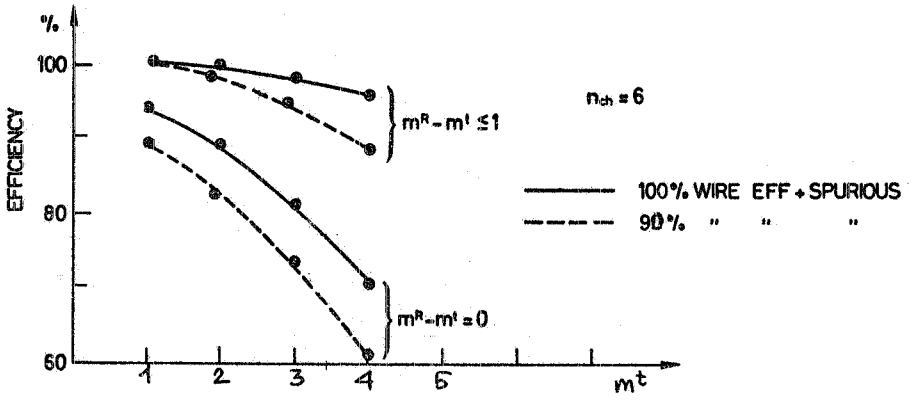

FIG. 12 - Effect of spurious sparks and wire inefficiencies on the event reconstruction efficiency for events with $n_{ch} = 6$.

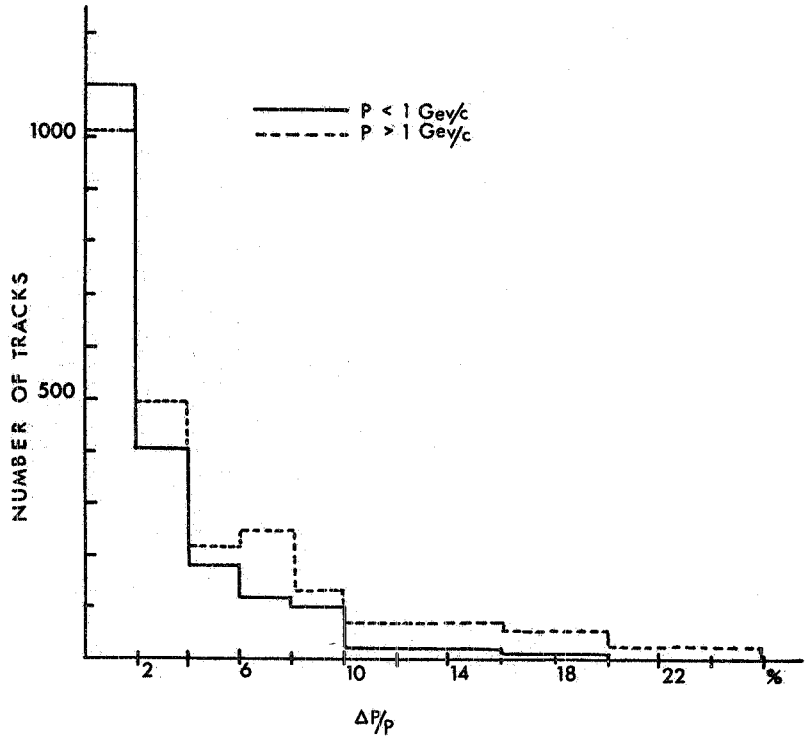

FIG. 13 - $\Delta p/p$ resolution in Vertex Detector.

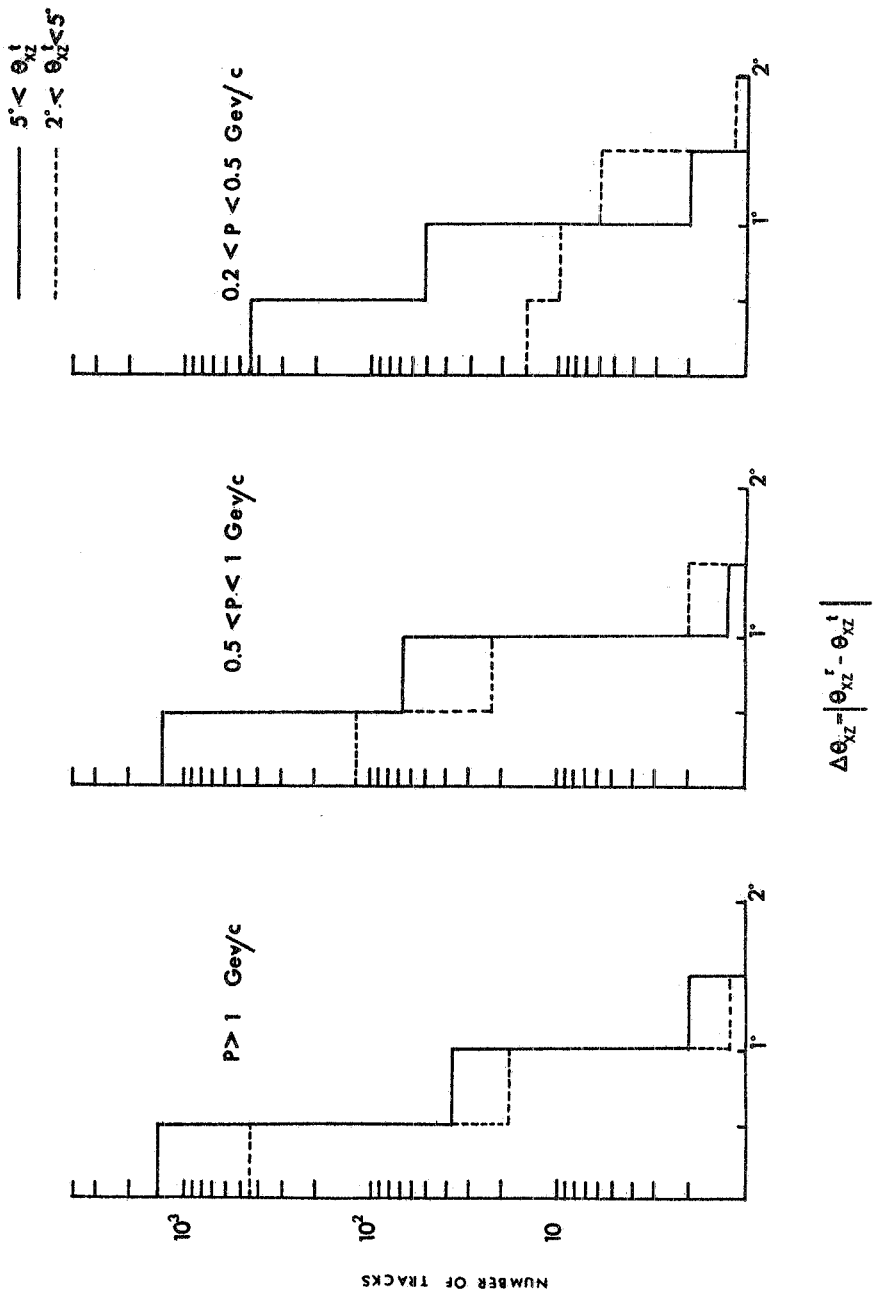

FIG. 14 - Plot of differences between the generated horizontal angle and the reconstructed one, $\Delta\theta_{xz} = |\theta^t_{xz} - \theta^r_{xz}|$, for three different ranges of particle momenta.

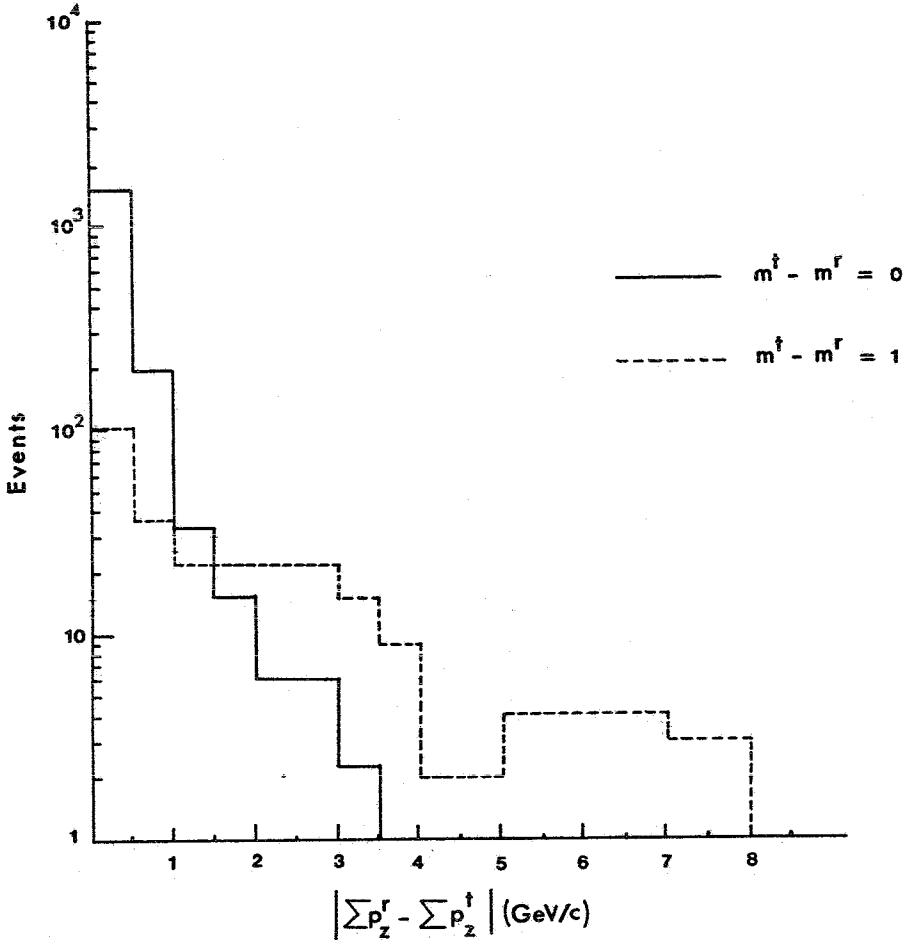

FIG. 15 - Plot of the differences between the true total longitudinal momentum and the reconstructed one of the particles of an event which are analyzed in the V.D. The full line represents fully analyzed events, the dotted line events with a missing track.

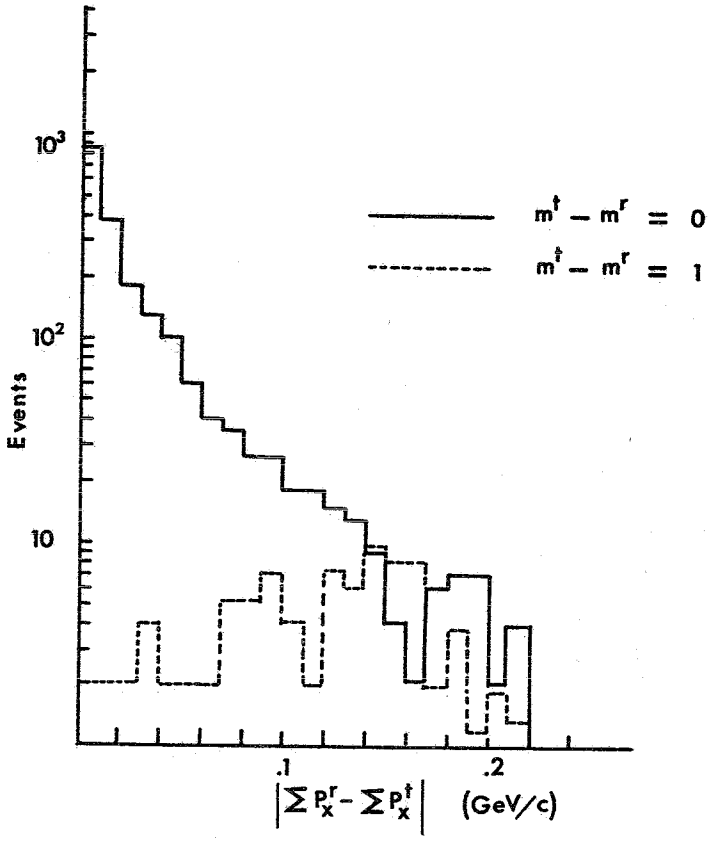

FIG. 16 - Same as Fig. 15 for transverse component of momentum.

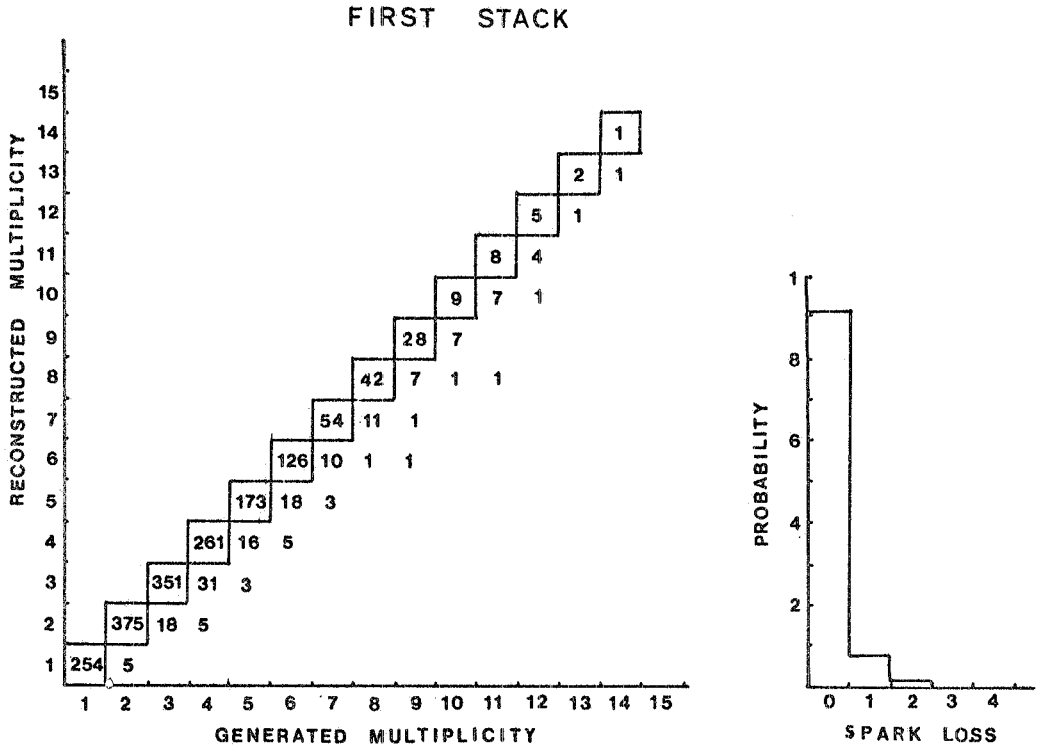

FIG. 17 - True multiplicity vs reconstructed multiplicity as measured in the first stack of drift chambers in the F.D.

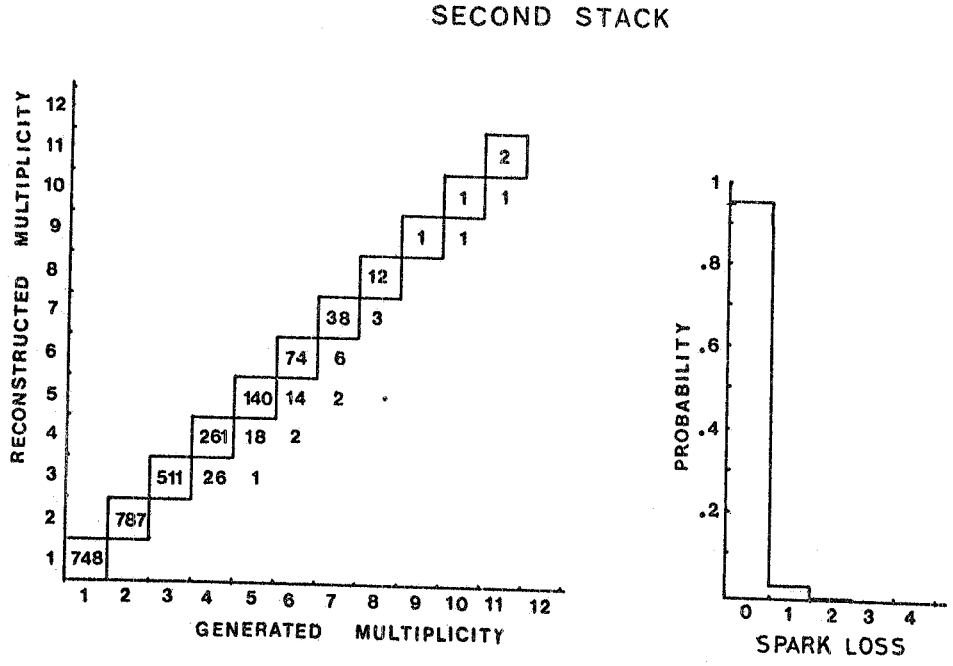

FIG. 18 - Same as Fig. 17 in the second stack.

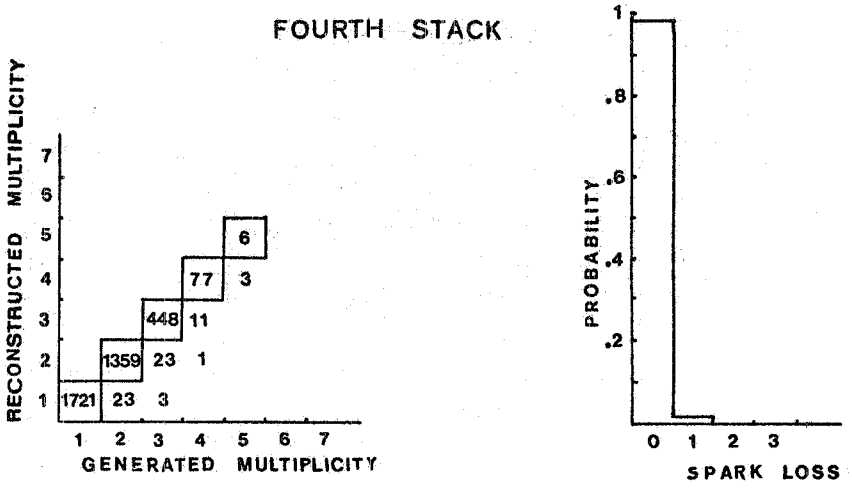

FIG. 19 - Same as Fig. 17 in the fourth stack.

re versus the number of true tracks crossing the chamber. For completeness, Fig. 20 gives the space resolution obtained under these conditions for correctly reconstructed sparks.

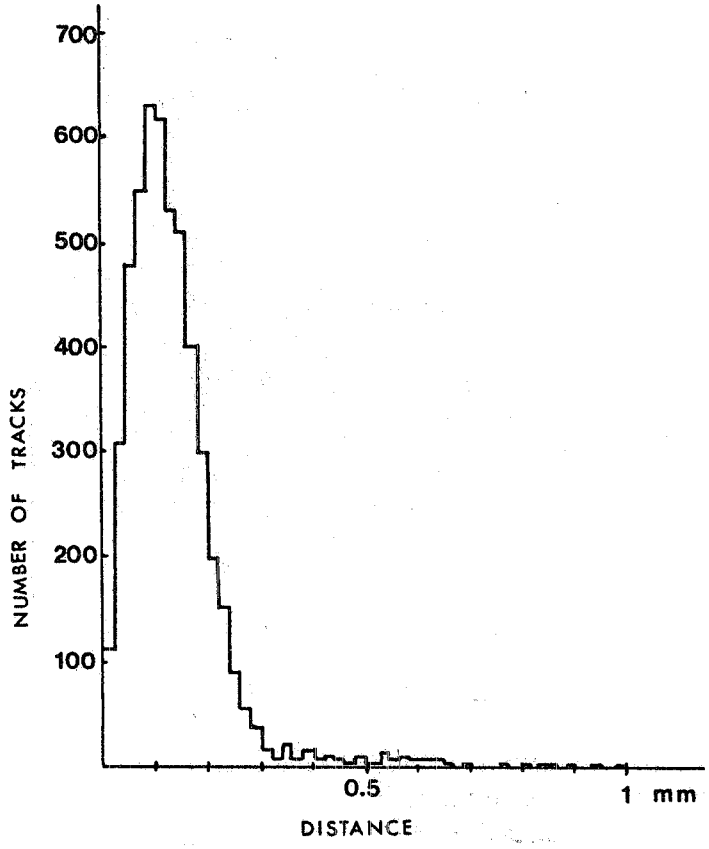

FIG. 20 - Drift chamber Monte Carlo spatial resolution.

In order to associate the hits in various chambers into tracks, the trajectories are first studied in the vertical plane, in which they are supposed to be straight lines. Since in this plane tracks never cross each other, we use this projection to trace them all back to the (common) origin. In this phase one makes use of the position of the interaction point as determined in the vertex detector. Groups of hits which are found aligned with the origin in the vertical plane are considered separately in the subsequent analysis in the horizontal plane. If some ambiguities are left over, such as a hit being compatible with two tracks, they are transferred to the horizontal plane routine and solved on the basis of a χ^2 analysis.

After the selection of good tracks coming from the target, the vertical projection analysis, using an unsophisticated routine, deals with the isolated points which can be due either to spurious firing of the wires or to particles not coming from the target. If these hits can be associated with straight lines we look for their origin and reject charged particles originated in interactions in the material of the spectrometer or in K^o decays. Possible isolated sparks left over at the end ot this analysis are neglected.

Because of the limited number of sparks per track (for each trajectory only the last two stacks of chambers crossed are examined) and because of its simplicity, the reconstruction routine in the forward spectrometer is highly efficient and fast. Figure 21 shows the number of good tracks that originated in the target and which are identified by the program, as a function of the generated event multiplicity. The resolution on the angle in the vertical plane for these tracks is shown in Fig. 22.

The projected trajectories in the horizontal plane are at first approximately determined by assuming for them a simple analytical expression. Different procedures are adopted according to the number and positions of measured hits. The tracks so determined are then used as the starting point of an iterative χ^2 analysis and the optimum projected angles and momenta are found. An ad hoc minimization routine allows the best fit value to be reached in three iterations on an average. The resolutions of θ_{xz} and $\Delta p/p$ are shown in Figs. 23a) and 23b).

5. - CONCLUSIONS. -

In this paper we have shown:

a) that with the apparatus previously described (LNF-74/7; CERN SPSC/6) and the proposed analysing procedure, the many-body events can be reconstructed with good accuracy up to multiplicity as high as about three times the average;
b) that an extended programme of physics can be carried out with an inclusive trigger and with additional triggers selecting particular

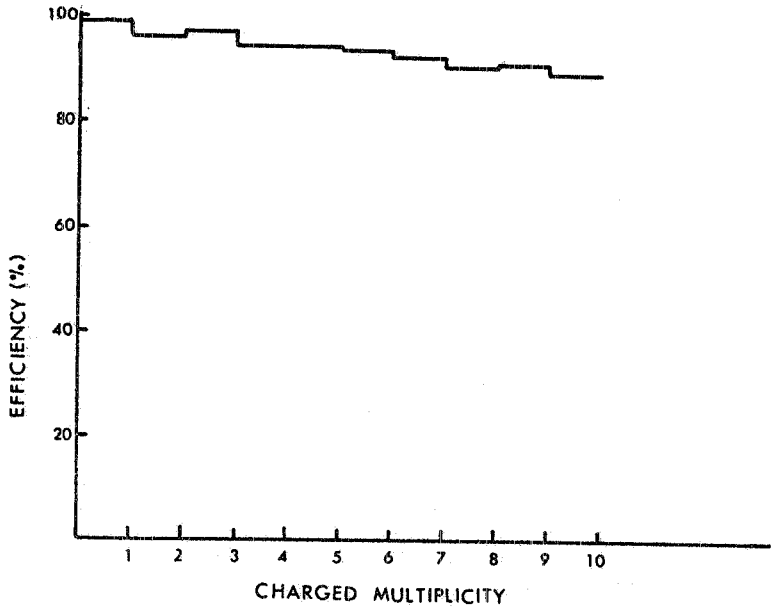

FIG. 21 - Efficiency of the reconstruction procedure using only the vertical projected plane as a function of event multiplicity.

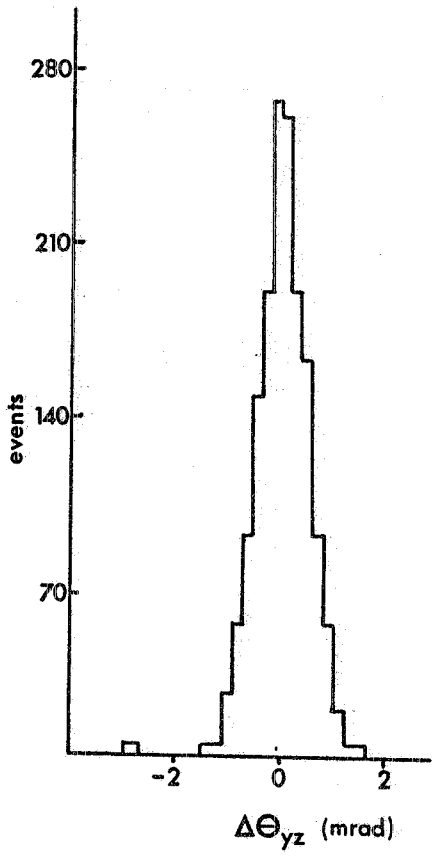

FIG. 22 - Vertical angle resolution at the forward spectrometer.

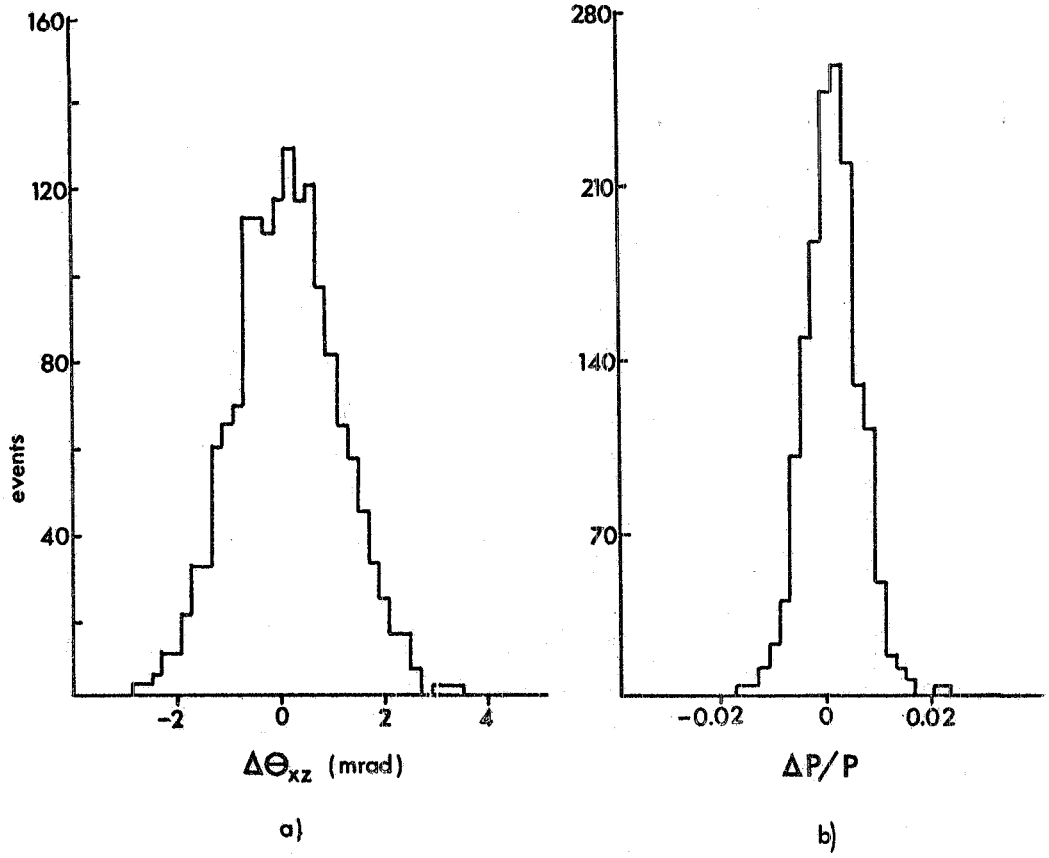

FIG. 23 - Horizontal angle resolution (a) and momentum resolution (b) of the forward spectrometer.

cathegories of events ;

c) that particle identtification is possible for particles to be used in the trigger and can be extended, if needed, to a large fraction of all charged secondaries.

We believe that these results substantiate an original claim that the proposed experiment is a realistic and fruitful approach to many body hadron physics.

APPENDIX I - Streamer Chamber. -

The dimensions of the streamer chamber that we plan to use are $100 \times 100 \times (2 \times 15)$ cm^3 (see Fig. A1.1); this chamber is placed inside the vertex magnet ($B \leq 15$ kG). The pulsed electric field, parallel to the magnetic field, is produced by a Blumlein line charged with 360 kV by means of a Marx-type generator. A charging time of $\sim$0.1-0.2 sec can be obtained.

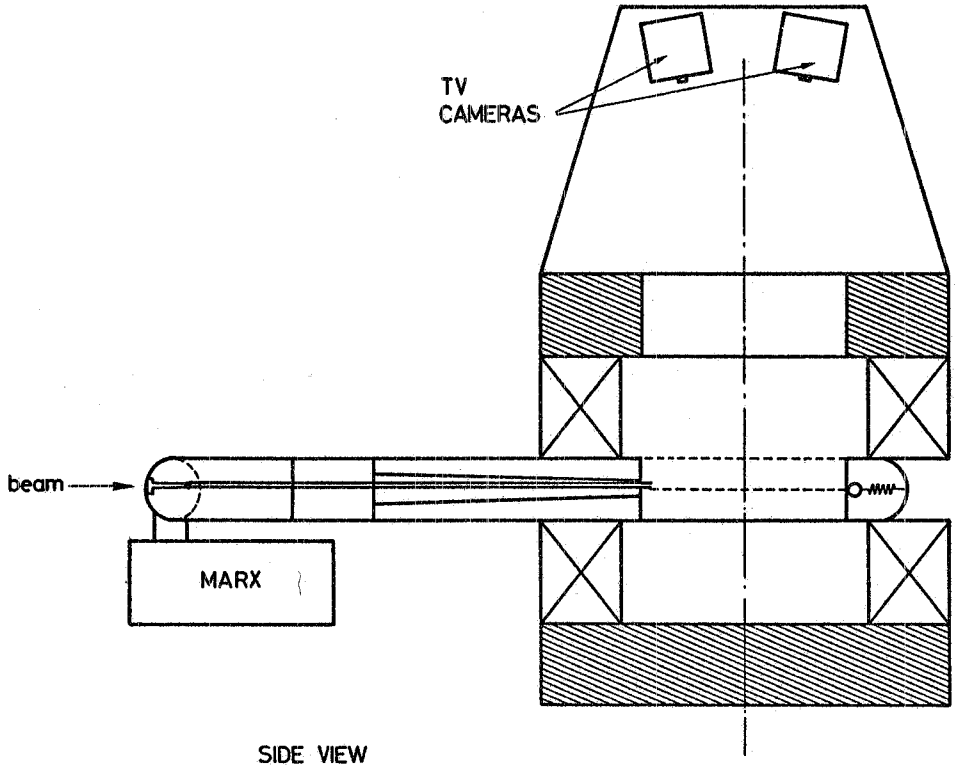

FIG. A.1.1. - Lay-out of streamer chamber.

A1.1. - Recording system. -

Two different recording systems are under consideration. By means of a usual photographic system (three cameras equipped with image intensifiers) a high sensitivity can be achieved, with an error on the position of $\sim$ 0.2 mm and on the ionization measurement for minimum ionizing particles of $\sim$15% (over a path of 50 cm)(*).

With a TV system we should have the advantages of a continuous check of the images, and also on-line digitized information. Very high quality TV tubes are now available, their sensitivity ranging from 0.6 mA/lm (VIDICON EEV 8521, 2000 TV lines) to 300 mA/lm (NOCTICON TH 9655, 750 TV lines). These figures are largely suf

(*) - CERN Yellow Report 74-4 (1974).

ficient for recording the light emitted by the streamers. In particular, a sensitivity of 0.06 mA/lm (PLUMBICON XQ 1020 R, 400 TV lines) is already adequate for recording the streamers of high luminosity(o). With the resolving power quoted above and a demagnification factor of 50, a setting error of 0.5-1 mm can be obtained. Further investigation on the detailed features of a TV system applied to a stream chamber are at present in progress.

A1.2. - Targets. -

The streamer chamber will be compatible with the use of different targets.

In the simplest case, helium gas at normal pressure will be used as a target and as a sensitive medium. Since the streamer chamber is planned for the study of the diffractive component, by selecting coherent events, it is necessary to recognize the recoiling α-particles from ^3He nuclei and to measure their momenta. The measurement of $|p|$ and θ can be performed by means of the usual techniques, giving the previsions quoted in Figs. A1.2 and A1.3, where a setting error of 0.5 mm was assumed and the dip angle was neglected.

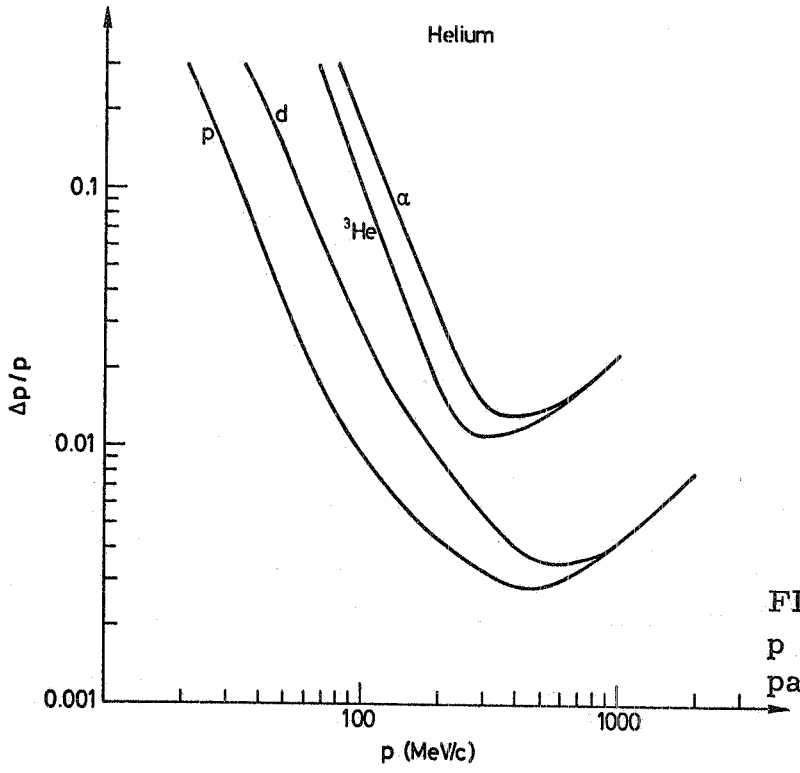

FIG. A1.2 - $\Delta p/p$ versus p in Helium for different particles.

(o) - Intern. Conf. on Instrumentation for High Energy Physics, Frascati (1973), p. 241.

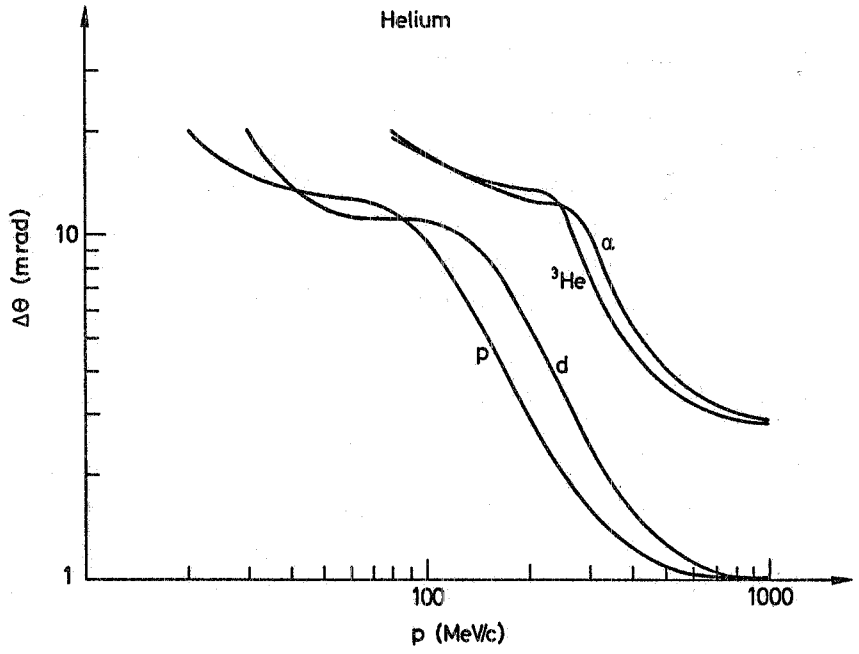

FIG. A1. 3. - Angular resolution versus p in Helium for different particles.

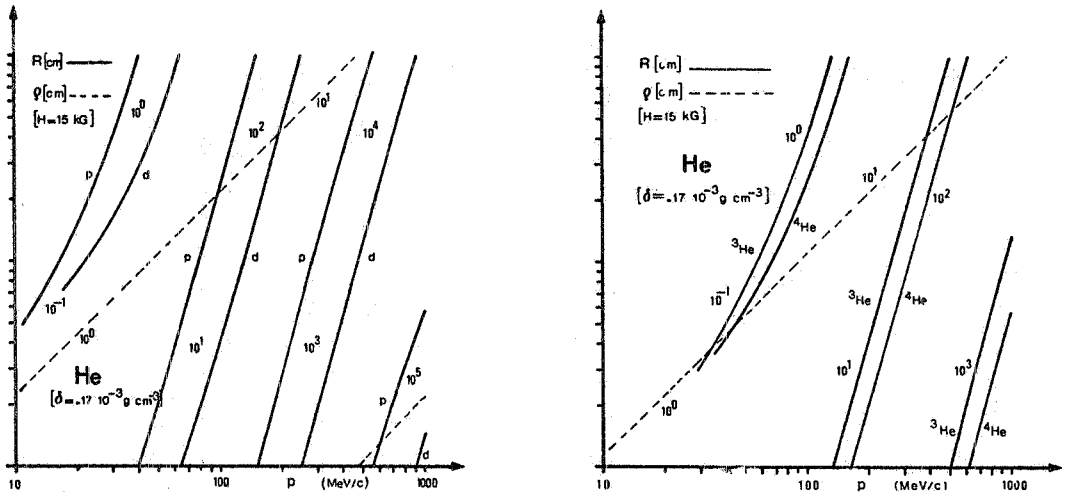

a) b)

FIG. A1. 4. - a) Range of protons and deuterons in Helium ; b) Same as a) for He^3 and He^4.

Two different situations are possible:

i) The α -particle remains inside the chamber ($|\vec{p}| < 300$ MeV/c) so that a measurement of the residual range R is sufficient. For a given value of $|\vec{p_\alpha}|$, the range of an ^{3}He nucleus is about twice the range of an α-particle (see Fig. A1.4). Figure A1.5 shows Δ R/R for α and ^{3}He nuclei in helium. For $|\vec{p}| > 100$ MeV/c the smallness of the percentage errors Δ p/p and ΔR/R allows an easy distinction of the two nuclei.

ii) For $|\vec{p_\alpha}| > 300$ MeV/c an ionization measurement becomes necessary. Since the ionization of an α-particle is about 1.5 times the ionization of a ^{3}He nucleus of the same momentum (see Figure A1.6), a reasonable discrimination can be obtained, provided that an error of less than 20% can be achieved in the ionization measurement. More accurate studies of this resolution for highly ionizing particles must still be performed.

The rate and background conditions, calculated by assuming a useful target length of 50 cm, a memory time of 200 μsec and a beam spill-out of 0.7 sec are given in Table A1.1.

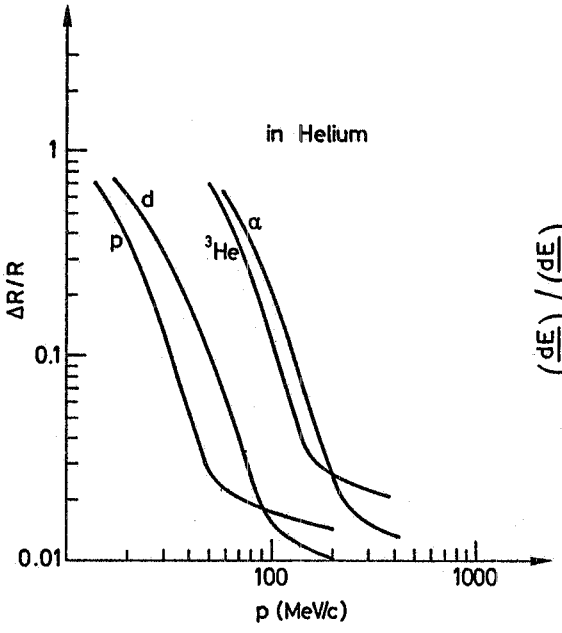

FIG. A1.5 - ΔR/R for different particles versus P in Helium.

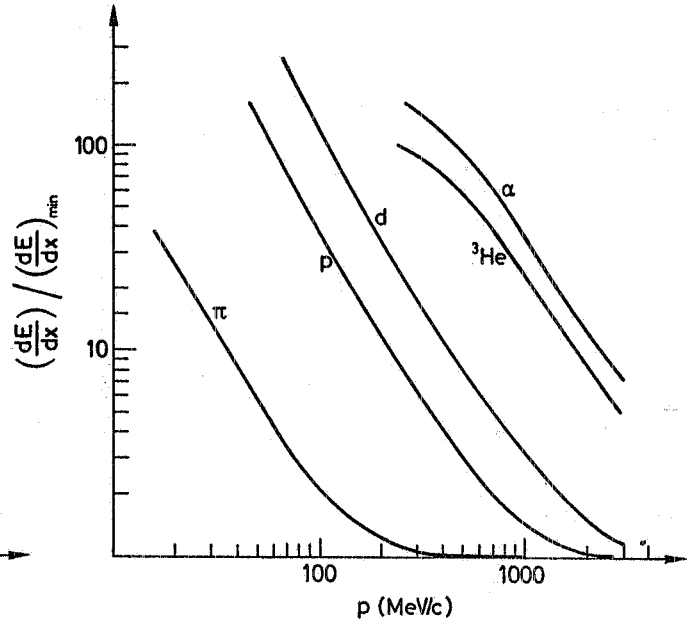

FIG. A1.6 - Energy loss normalized to a minimum ionizing particle versus p.

Target	Sensitive medium	Minimum detectable momentum (MeV/c)	Luminosity ($cm^{-2}\,sec^{-1}$)	Beam intensity	Rate (mb)	Probability of spurious events (%)
He	He	100	6×10^{26}	5×10^{5}	0.6	2
H_2 (liquid)	He	180	10^{28}	10^{5}	10	3
H_2 (gas)	He	50	2.5×10^{27}	10^{6}	2.5	2
H_2 (gas)	H_2 (gas)	20	2.5×10^{27}	10^{6}	2.5	2

TABLE A1.1

For hydrogen and deuterium we can use a gaseous or a liquid target positioned inside a helium streamer, as has already been done in several experiments(x). Resolution and notes have been calculated by assuming a liquid H_2/D_2 target of 5 cm length and 1 m diameter, with a wall thickness of 0.1 mm, and a gaseous H_2/D_2 target at atmospheric pressure, of 50 cm length, 1 cm diameter, and 25 μ wall thickness. The most relevant difference between the two targets is the cut in recoil momentum due to the material in the target itself and in the walls. Figure A1.7 shows the momentum of the proton emerging from the target (p_{em}) as a function of the production angle for both targets. The same plot is shown in Fig. A1.8 for deuterons.

A comparison of the performances of liquid and gaseous targets is given in Table A1.1. The values of $\Delta p/p$, $\Delta\theta$, and $\Delta R/R$ for protons and deuterons in helium are given in Figs. A1.2, A1.3, and A1.5, respectively.

Recoiling protons of known momentum, below $p \sim 1$ GeV/c, can be separated from pions by means of dE/dx measurement in the trigger counters positioned between the coils of the magnets, or by range measurement if the proton trajectory is contained in the chamber. The same criteria can be applied to the identification of deuterons.

(x) - Int. Conf. on Instrumentation for High-Energy Physics, Frascati (1973), p. 115.

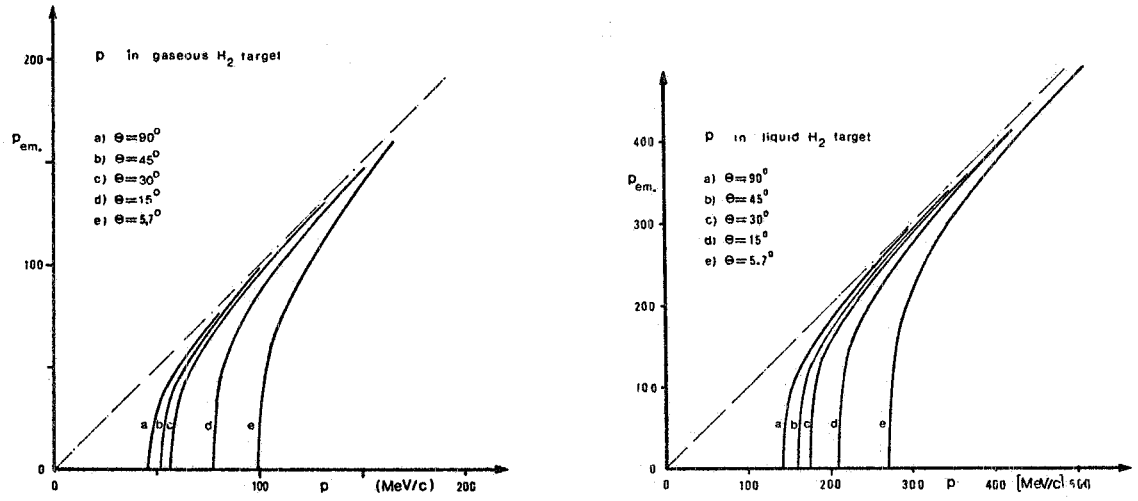

FIG. A. 1. 7 - Momentum of emerging proton versus original momentum for various production angles in gasseous and liquid H_2 target.

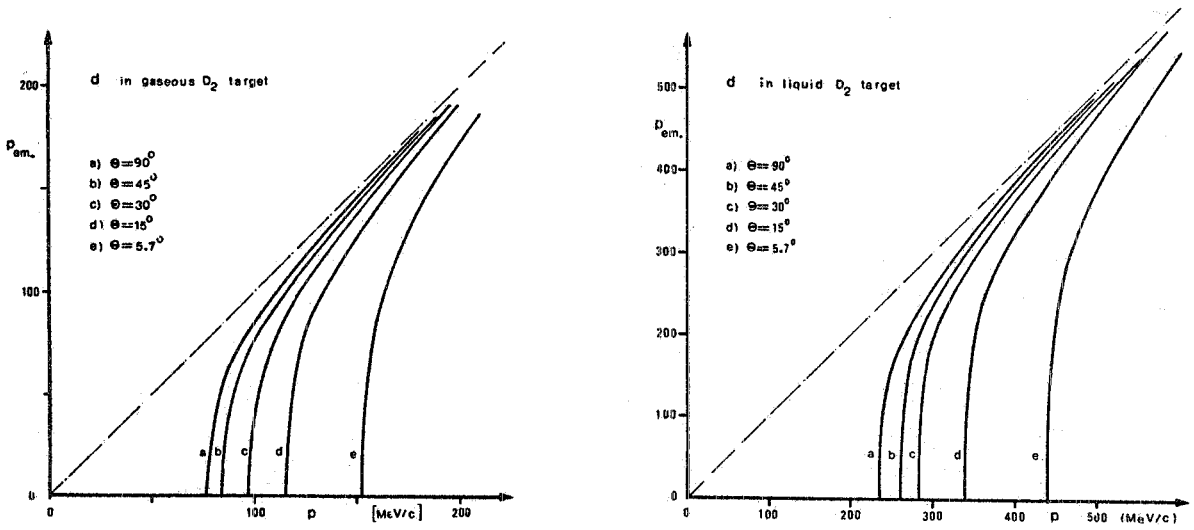

FIG. A. 1. 8 - Same as Fig. A. 1. 7 for D_2 target.

A1.3. - Use of an H_2/D_2 streamer chamber. -

The operation of an H_2 streamer chamber has already been attempted several times(1).

A study is in progress inside our collaboration to check whether the ultraviolet radiation produced by the streamers in hydrogen can be utilized with results comparable to those obtained with helium streamer chambers in the visible range(2). The advantage of this chamber would be to further reduce the minimum detectable value of the proton momentum to about 20 MeV/c. The same chamber could then be operated with D_2 gas for coherent production on deuterons. Also the momentum angle, and range resolution would be improved by at least a factor of 2, as shown by Fig. A1.9. Range measurements would allow also an easier identification of protons and deuterons in deuterium (Rd/Rp $\sim$ 5 at fixed momentum).

The structure of this chamber would, however, be more complicated. For instance, only mirrors can be used in the optics, instead of lenses. Also the use of special ultra-violet TV tubes is required. Photons between 1050 and 3000 Å are detected by a TH 9301 tube and converted into visible light with a gain of a factor of 10. If used together with a TH 9892 it provides a sensitivity of 0.25 mA/lm and a resolution of 250 TV lines.

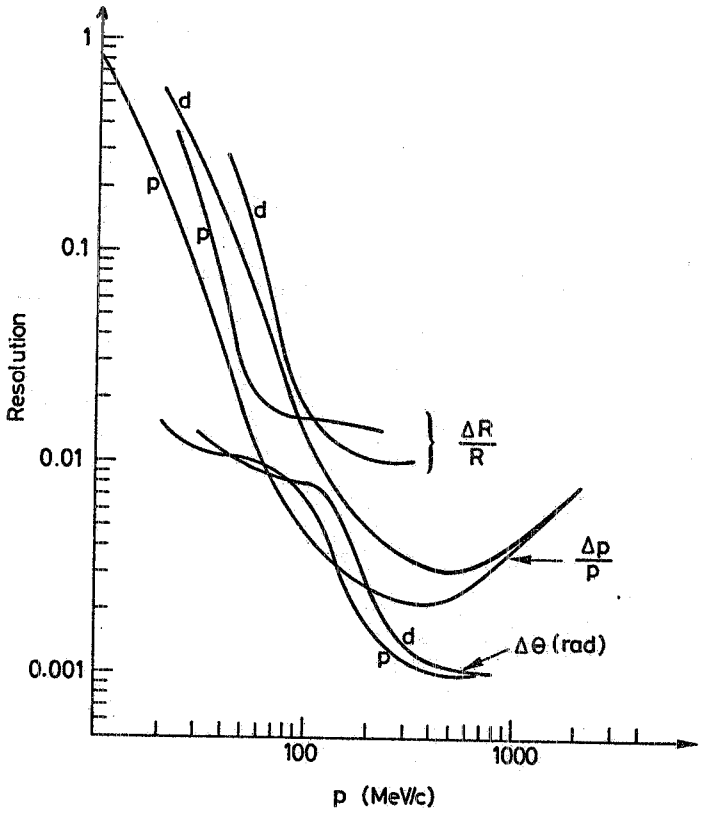

FIG. A.1.9 - Range momentum and angle resolution for different particles.

(1) - F. Rohrbach et al., Nuclear Instrum. Methods 3, 485 (1973).
(2) - M. Severi et al., Rome Institute report I.F.U. 537/1974.

APPENDIX 2 - Silicon Detector. -

The silicon detector target, as a device for rejecting incoherent event, has already been used successfully in coherent production experiments[1, 2], and detailed accounts of its characteristics can be found in the literature. It consists basically of an arrangement of very thin silicon sheets surrounded by an anticoincidence scintillator in order to eliminate the charged recoils at large angles.

The underlying principle of the silicon target operation is that at a fixed momentum transfer the recoil nucleus releases in the detector an energy 28 times smaller than that of recoiling proton. This fact together with the anticoincidence criteria that reject also the events where a proton is evaporated at large angle near the surface of the detector, allows the rejection of essentially all the incoherent events in which the nucleus breaks up by emitting protons.

Because of the very good energy resolution of the detector it is then possible to measure the invariant momentum transfer $|t|$ to very low values of $|t|$ thus selecting a kinematical region where the coherent production largely dominates. The incoherent background, mainly due for the cases in which the nucleus breaks up by emitting only neutrons, is almost of the order of a few per cent in the region of the first diffractive maximum. The t' distributions shown in Fig. A2.1a and A2.1b and which refer to data taken in a previous experiment[1, 2], give an impressive look of the incoherent background reduction obtained by means of the silicon detector target[3].

The background is reduced by a factor of 2 in the region of the forward peak [$t' < 0.03$-$(GeV/c)^2$] and by a factor of 4 in the region of the second maximum.

In Table A2.1 we summarize some of the main physical and technical characteristics of our proposed silicon detector target for the SPS experiment. Owing to the short time constant operation of the electronic chain, the silicon detector signal can be used directly in the trigger of the experiment.

---

(1) - C. Bemporad et al., Nuclear Phys. B 33, 397 (1971).
(2) - C. Bemporad et al., Nuclear Phys. B 42, 627 (1972).
(3) - G. Bellini et al., Nuclear Instrum. and Methods 107, 85 (1973).

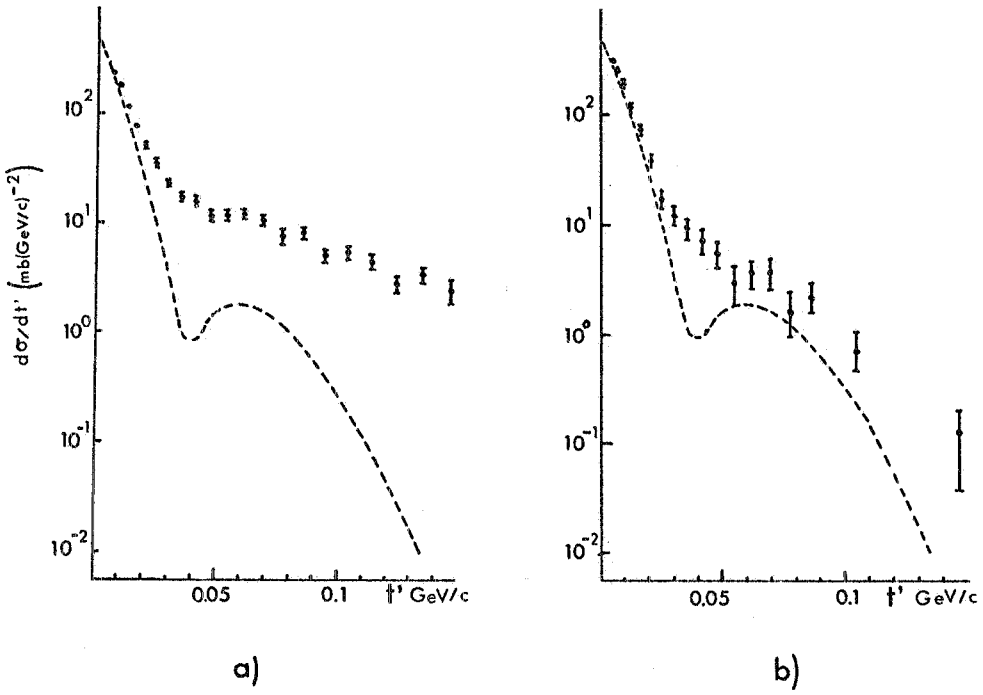

FIG. A2.1 - The t' distribution refer to data taken in previous experiments (Footnote 1, 2, 3 of Appendix 2).

No. of silicon sheets	10
Thickness of a silicon sheet	200 μ
Electronic noise	20 keV
Energy resolution	{ 70 keV (for 3π) 140 keV (for 5π)
|t| resolution	0.004 $(GeV/c)^2$
Total pulse width	100 nsec

TABLE A.2.1